

---

# StableTTA: Improving Vision Model Performance by Training-free Test-Time Adaptation Methods

---

**Zheng Li**

Department of Computer Science  
New York Institute of Technology  
zli66@nyit.edu

**Jerry Cheng**

Department of Computer Science  
New York Institute of Technology  
jcheng18@nyit.edu

**Huanying Helen Gu**

Department of Computer Science  
New York Institute of Technology  
hgu03@nyit.edu

## Abstract

Ensemble methods improve predictive performance but often incur high memory and computational costs. We identify an aggregation instability induced by nonlinear projection and voting operations. To address both efficiency challenges and this inconsistency, we propose StableTTA, a training-free test-time adaptation method with two variants. StableTTA-I targets coherent-batch inference settings, where temporally or semantically adjacent observations are likely to belong to the same class. Examples include burst photography, video streams, robotics perception, and industrial inspection. Under coherent-batch inference, StableTTA-I substantially improves prediction consistency and accuracy through variance-aware logit aggregation. StableTTA-II establishes feature-level cropping, enabling efficient logit aggregation with a single forward pass on a single model backbone. Experiments on ImageNet-1K across 71 models demonstrate that StableTTA-I consistently improves prediction accuracy under coherent-batch inference, while StableTTA-II provides lightweight and architecture-agnostic accuracy improvements with minimal computational overhead. These results suggest that inference-time semantic coherence and aggregation stability provide useful perspectives for improving practical test-time adaptation systems.

## 1 Introduction

Ensemble methods improve predictive robustness by aggregating multiple predictions [6, 1]. However, their practical adoption is limited by substantial memory and computational overhead, since inference cost typically scales linearly with the number of experts. Test-time augmentation (TTA) partially alleviates this issue by applying multiple augmentations to a single model [14], but still requires repeated forward passes and therefore remains computationally expensive.

In this work, we examine the limitations of ensemble methods and identify an inherent aggregation inconsistency between different aggregation strategies. While conventional image classification assumes independently sampled test examples, many real-world deployment scenarios exhibit strong local semantic consistency. For example, consecutive video frames, burst photographs, robotic observations, medical slices, and industrial inspection streams often contain correlated views of the same semantic object or category. In these settings, neighboring samples provide contextual information that is ignored by standard test-time augmentation methods. We refer to this setting as *coherent-batch inference*, where semantically adjacent observations are processed jointly during

Table 1: Representative inference regimes in visual recognition systems.

Regime	Assumption	Example Applications
IID inference	Independent samples	Standard image classification
Coherent-batch inference	Neighboring samples correlated	Burst imaging, inspection
Multi-view inference	Multiple views of same object	3D recognition
Sequential inference	Temporal continuity	Video and robotics

inference. More generally, inference settings in visual recognition systems can be categorized according to the statistical relationships among test observations. While most existing image classification benchmarks and test-time adaptation methods assume independently sampled inputs, many practical deployment scenarios exhibit structured dependencies across observations. To better position our setting, Table 1 summarizes several representative inference regimes commonly encountered in visual recognition systems. Most existing TTA methods are developed primarily for IID inference, whereas StableTTA-I explicitly exploits deployment-time semantic coherence during aggregation.

Motivated by these observations, we propose StableTTA, a training-free test-time adaptation framework consisting of two complementary methods. StableTTA-I targets coherent batch inference and introduces a consensus-preserving logit-aggregation strategy for semantically correlated observations. Under coherent-batch inference, StableTTA-I substantially improves prediction consistency and accuracy. StableTTA-II addresses the computational limitations of conventional ensemble methods by introducing feature-level cropping, enabling multiple predictions from a single backbone forward pass with only negligible additional computation in the lightweight classification head.

## 2 Related Work

For image classification, model averaging is an ensemble strategy widely used to improve performance in general settings [6]. As introduced by Breiman [1], the outputs of multiple independently pretrained models are typically aggregated by majority voting on the predictions or averaging the predicted probabilities. In general, although model averaging can provide modest performance gains, these improvements are often marginal relative to the substantial increase in resource requirements [7, 33]. Furthermore, both the total number of parameters and the computational cost (FLOPs) grow additively with the number of models. As a result, model averaging is typically less efficient than training a well-optimized single model [7].

As a partial solution, TTA uses a single model to reduce the total number of model parameters. Specifically, it applies a set of data augmentations (e.g., flipping, cropping) to an input image and feeds the augmented images into the same model to produce multiple logits for aggregation [14, 7], while maintaining a fixed model size. However, it still incurs additional inference-time computation. For instance, ResNet [7] and DenseNet [10] employ a 10-crop data augmentation during validation, leading to a tenfold increase in FLOPs. As a result, TTA typically yields only a modest improvement, often no more than 2% in top-1 accuracy [28, 13, 15].

Although TTA has been widely adopted, relatively few works have gained significant attention in top-tier venues, primarily because its key limitation—the **significant increase in computational cost**—remains unresolved [29].

Historically, progress in large-scale visual recognition benchmarks such as ImageNet-1K (1.28M images) [3] has been characterized by incremental improvements, with successive model generations typically achieving only 1%–2% gains in top-1 accuracy [14, 30, 7, 33, 4]. While some models report accuracies exceeding 85% [4, 18], these gains are often enabled by scaling training data using larger external datasets such as ImageNet-21K (14M images) [26] and JFT-300M (300M images) [22], highlighting the role of data scale in achieving state-of-the-art performance.

### 3 Background

For a better understanding of the most commonly used ensemble methods, consider a  $C$ -class classification task. Let logit vector  $\mathbf{z}$  denote the outputs of a model  $f$  with parameters  $\theta$  for input  $\mathbf{x}$ :

$$\mathbf{z} = f(\mathbf{x}; \theta) \in \mathbb{R}^C.$$

After applying the softmax function, we obtain the probability distribution  $\mathbf{p}_\theta(y | \mathbf{x})$  of class  $y$  over the  $C$  classes:

$$\mathbf{p}_\theta(y = k | \mathbf{x}) = \frac{\exp(\mathbf{z}_k)}{\sum_{j=1}^C \exp(\mathbf{z}_j)}, \quad k = 1, \dots, C.$$

The predicted class is given by

$$\hat{y} = \arg \max_k \mathbf{z}_k = \arg \max_k \mathbf{p}_\theta(y = k | \mathbf{x}).$$

*Hard voting*, *soft voting*, and *logit averaging* are common aggregation strategies in ensemble methods [6, 23]. Among them, logit averaging is generally more effective for single-model ensembles (see Appendix A, Table 4). For an ensemble of  $N$  experts, the aggregation can be formulated as follows:

- **Hard Voting** (as illustrated by orange blocks in Fig. 1a): After all  $N$  votes are cast as  $\{\hat{y}^{(1)}, \hat{y}^{(2)}, \dots, \hat{y}^{(N)}\}$ , the most favorable class is selected as:

$$\hat{y}_{\text{hard}} = \arg \max_k \sum_{i=1}^N \mathbb{1}_{\hat{y}^{(i)}=k}.$$

- **Soft Voting** (as illustrated by cyan blocks in Fig. 1a): After class probabilities from the  $N$  forward passes are averaged, the class with the highest mean probability is selected. Specifically, in the case of multi-model ensembles with models  $\{f(\cdot; \theta^{(i)}) | i = 1, \dots, N\}$ , we have

$$\hat{y}_{\text{soft}} = \arg \max_k \frac{1}{N} \sum_{i=1}^N \mathbf{p}_{\theta^{(i)}}(y = k | \mathbf{x}).$$

In the case of TTA with a single model  $f(\cdot; \theta)$  and augmentation policies  $\{\psi^{(i)} | i = 1, \dots, N\}$ , we have

$$\hat{y}_{\text{soft}} = \arg \max_k \frac{1}{N} \sum_{i=1}^N \mathbf{p}_\theta(y = k | \psi^{(i)}(\mathbf{x})).$$

- **Logit Averaging** (as illustrated by orange blocks in Fig. 1a): After logits are averaged across  $N$  forward passes, the class with the highest mean logit is selected as:

$$\hat{y}_{\text{logit}} = \arg \max_k \frac{1}{N} \sum_{i=1}^N \mathbf{z}_k^{(i)}.$$

**Limitations** Model averaging requires storing multiple models, and its inference-time cost equals the sum of all models. In contrast, TTA uses a single model but still incurs an  $N$ -fold increase in inference-time cost. Both methods yield only modest improvements. To better illustrate this, Fig. 6 in Appendix A compares the pipelines of a single-model one forward pass, multi-model averaging, and TTA.

**Aggregation Inconsistency** In ensemble methods, different aggregation strategies can yield inconsistent results. For example, as illustrated in Fig. 1b, given three logit vectors  $(\mathbf{z}^{(1)}, \mathbf{z}^{(2)}, \mathbf{z}^{(3)})$ , the aggregated predictions are inconsistent: 3 from hard voting, 2 from soft voting, and 1 from logit averaging. We also observe that when the logits  $\{\mathbf{z}^{(1)}, \mathbf{z}^{(2)}, \dots\}$  are sparsely distributed, the nonlinearity and non-bijective nature of the softmax and indicator functions can amplify the differences among them. In contrast, when the logits are more densely clustered, different aggregation strategies are more likely to yield consistent predictions. We provide both theoretical analysis and empirical evidence in Appendix C and D to support this observation. The empirical results are well fitted by our derived relationship between  $P(\hat{y}_{\text{logit}} \neq \hat{y}_{\text{hard}})$  and  $\text{Var}(\mathbf{z})$ . In summary, reduced variance leads to more inconsistencies.

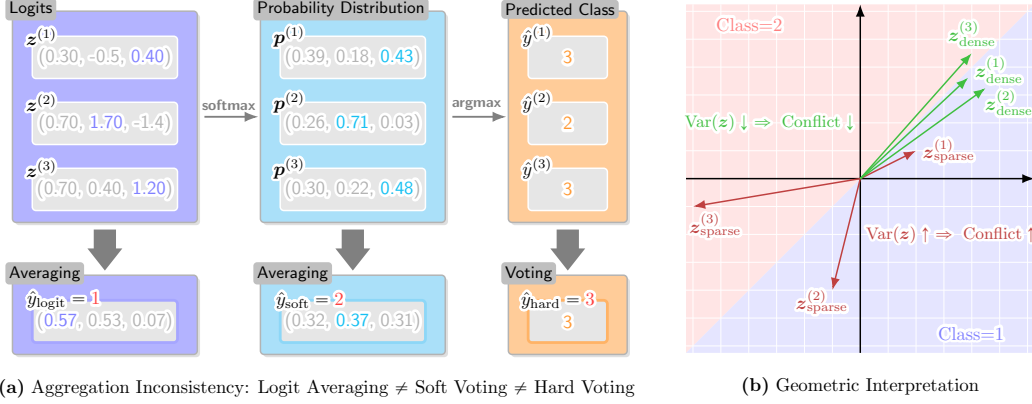


Figure 1: (a) **Aggregation Inconsistency:** Given branch logits  $\{z^{(i)} \mid i = 1, 2, 3\}$ , probabilities  $p^{(i)} = \text{softmax}(z^{(i)})$ , and predictions  $\hat{y}^{(i)} = \text{argmax } p^{(i)}$ , different aggregation strategies may produce inconsistent results. Here, logit averaging predicts  $\hat{y}_{\text{logit}} = 1$ , soft voting predicts  $\hat{y}_{\text{soft}} = 2$ , and hard voting predicts  $\hat{y}_{\text{hard}} = 3$ . (a) **Explanation:** When  $(z^{(1)}, z^{(2)}, \dots)$  are sparsely distributed, inconsistency  $\hat{y}_{\text{logit}} \neq \hat{y}_{\text{soft}} \neq \hat{y}_{\text{hard}}$  are more likely due to the nonlinearity and non-bijection of softmax. In contrast, when the logits are more densely clustered, such inconsistencies are less likely.

## 4 Method

### 4.1 StableTTA-I

As discussed in Section 1, StableTTA-I targets coherent-batch inference, where neighboring observations exhibit strong semantic correlation and therefore provide complementary predictive evidence during aggregation. Formally, let  $(x_i, y_i)$  denote sequential observations. We assume there exists a locality scale  $\delta > 0$  such that

$$P(y_i = y_j \mid |i - j| < \delta) \gg \frac{1}{C}$$

where  $C$  denotes the number of classes. This assumption implies that neighboring samples are substantially more likely to share the same semantic category than under IID sampling.

Under this setting, aggregation stability becomes particularly important because predictions from neighboring observations and augmented samples are jointly combined during inference. As discussed in Section 3, aggregation inconsistency arises because averaging in the logit, probability, and label spaces yields different behaviors after nonlinear projection via the softmax/argmax functions.

Motivated by this observation, we introduce a consensus-preserving logit post-processing operator called Non-Significant Suppression (NSS), which suppresses unstable low-confidence posterior modes prior to aggregation:

$$\text{NSS}(z, K) := z \odot \mathbf{1}_{\text{TopK}(z, K)} + \min(z) \cdot (\mathbf{1} - \mathbf{1}_{\text{TopK}(z, K)}), \quad K = 1, \dots, C \quad (1)$$

where,  $\mathbf{1}$  is the all-ones vector,  $\mathbf{1}_{\text{TopK}(z, K)} \in \{0, 1\}^C$  is the indicator vector of the Top- $K$  indices (equal to 1 for indices in the Top- $K$  set and 0 otherwise), and  $\odot$  denotes element-wise multiplication. In this work, we apply NSS to logit averaging and prove it reduces  $\text{Var}(z)$ .

From the definition of NSS, we have:

$$\text{NSS}(z, K)_i = \begin{cases} z_i, & i \in \text{TopK}(z, K), \\ \min(z), & i \notin \text{TopK}(z, K), \end{cases}$$

and

$$\frac{\partial}{\partial z_j} \text{NSS}(z, K)_i = \begin{cases} 1, & \text{if } i \in \text{TopK}(z, K) \text{ and } i = j, \\ 0, & \text{if } i \in \text{TopK}(z, K) \text{ and } i \neq j, \\ 1, & \text{if } i \notin \text{TopK}(z, K) \text{ and } j = \arg \min z, \\ 0, & \text{if } i \notin \text{TopK}(z, K) \text{ and } j \neq \arg \min z. \end{cases}$$

Hence, almost everywhere,

$$\|\nabla \text{NSS}(\mathbf{z}, K)_i\|^2 = \sum_{j=1}^C \left( \frac{\partial}{\partial z_j} \text{NSS}(\mathbf{z}, K)_i \right)^2 = 1.$$

Our experiments in Appendix C and D show that, under our proposed augmentation policy and image sampling strategy, in most cases there exist  $\mu_i$  and  $\sigma$  such that  $\mathbf{z}_i \sim \mathcal{N}(\mu_i, \sigma^2)$ . Applying the Gaussian Poincaré inequality, we obtain

$$\text{Var}(\text{NSS}(\mathbf{z}, K)_i) \leq \mathbb{E} \left[ \sigma^2 \|\nabla \text{NSS}(\mathbf{z}, K)_i\|^2 \right] = \sigma^2 = \text{Var}(\mathbf{z}_i).$$

This implies that NSS reduces the variance of the logit vector  $\mathbf{z}$ , thereby further avoiding the prediction inconsistency described in Section 3. Furthermore, it is important to note that

$$\text{NSS}(\mathbf{z}, C) = \mathbf{z} \odot \mathbf{1} + \min(\mathbf{z}) \cdot (\mathbf{1} - \mathbf{1}) = \mathbf{z},$$

which implies that when  $K = C$ , StableTTA-I is downgraded to the conventional TTA method.

To further reduce variance, we reformulate mixup [42] and CutMix [40] under the constraint that images within each batch mostly belong to the same class (see Appendix B). Although this image sampling strategy restricts the scope of applicability (e.g., requiring multiple captures of the same object for StableTTA-I), it yields substantial improvements in model performance.

In summary, StableTTA-I uses the following representation to replace the logits  $\mathbf{z}$ :

$$\mathbf{z} \leftarrow \frac{1}{N} \sum_{i=1}^N \text{NSS}(f(\psi^{(i)}(\mathbf{x}); \boldsymbol{\theta}), K).$$

In Section 5.1, we present an overview of the comparison experiments, ablation studies, and sensitivity analysis. A complete comparison with conventional TTA methods (under the same image sampling strategy as ours) is provided in Appendix F. In order to empirically demonstrate that NSS can mitigate the inconsistency, we provide detailed ablation studies in Appendix G, which show that, under the same sampling strategy and augmentation policy, applying NSS improves model performance. Additional results on sensitivity analysis are reported in Appendix H. Appendix I presents the statistical significance of the experimental results.

## 4.2 StableTTA-II

In this section, we present StableTTA-II, designed to address the limitations discussed in Section 3.

To ensure unchanged memory usage and minimal additional computational cost, we constrain our method to a single model and a single forward pass for logit aggregation. This contrasts with conventional test-time augmentation (TTA), which requires multiple forward passes and incurs significantly higher computational cost. To achieve this goal, we do not apply input augmentations to generate multiple logits, as doing so would scale the total FLOPs (see Appendix A, Fig. 6). Instead, we apply feature-level cropping to produce multiple logits (see Fig. 2).

In general, most of the computational cost (FLOPs) lies in the model backbone. Although the head is executed multiple times, the overall FLOPs remain nearly unchanged. For example, consider the ResNet-50 architecture with a single  $224 \times 224$  input resolution: the backbone consists of conv + bn/relu/maxpool + residual blocks 1–4, totaling 4.087 GFLOPs, while the head consists of avgpool + flatten + linear, totaling 0.002 GFLOPs. Accordingly, StableTTA-II achieves a single forward pass on the main backbone while introducing a negligible increase in overall computational cost.

We decompose the model  $f$  into a feature extractor (backbone) and a classification head, such that

$$f(\mathbf{x}) = \text{Head} \circ \text{Backbone}(\mathbf{x}).$$

Specifically, as illustrated in Fig. 2, StableTTA-II modifies the standard inference pipeline by introducing feature-level **deterministic** cropping and logit aggregation:

$$\bar{\mathbf{z}} = \frac{1}{N} \sum_{i=1}^N \text{Head}(\text{crop}^{(i)}(\text{Backbone}(\mathbf{x}))).$$

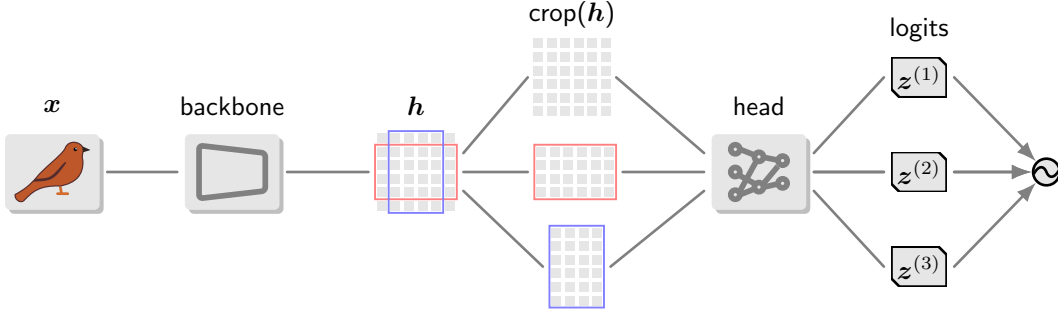


Figure 2: Illustration of StableTTA-II. Given an input image  $x$ , the backbone produces a feature representation  $h$ . Multiple deterministic crops are sampled at the feature level and processed by a shared head to obtain multiple logits  $\{z^{(i)}\}$ , which are aggregated to form the final prediction.

As an example, we define the crops on the ResNet feature map  $h = \text{Backbone}(x)$  as:

$$\text{crop}^{(0)}(h) = h, \quad \text{crop}^{(1)}(h) = h[k : -k, :], \quad \text{crop}^{(2)}(h) = h[:, k : -k].$$

where  $k$  corresponds to approximately 6.25% ( $= 1/2 \times (256 - 224)/256$ ) of the feature map size along each spatial dimension. This choice is consistent with common practice in ImageNet-trained models, where an 87.5% ( $= 1 - 2 \times 6.25\%$ ) crop ratio is typically adopted during both training (random cropping) and evaluation (center cropping).

In Section 5.2, we present a detailed analysis of model performance gains using StableTTA-II. The theoretical analysis of computational cost, model head configurations, and feature-level cropping settings are provided in Appendix J. In Appendix K, we conduct a sensitivity analysis to explore other feature-level augmentations. These experiments show that random cropping and random erasing degrade the final predictions, reducing accuracy below that of the base model.

## 5 Experiments

We evaluate StableTTA in terms of accuracy, memory usage, and computational cost. First, we compare StableTTA across a wide range of ImageNet-1K models. We then show that StableTTA-I enables lightweight architectures to outperform larger models in top-1 accuracy while maintaining favorable efficiency–performance trade-offs. We further present ablation studies and sensitivity analysis to examine the effectiveness and robustness of the proposed methods. Finally, we demonstrate consistent performance improvements achieved by StableTTA-II and provide additional analysis.

**Dataset.** ImageNet-1K [3] is a commonly used and highly challenging benchmark dataset, which we adopt for evaluation. It contains 1.28 million training images and 50,000 validation images across 1,000 categories. Over the past years, widely accepted models have typically achieved only incremental improvements of 1%–2% in top-1 accuracy per advancement [14, 30, 7, 33, 4].

**Models.** All pretrained models used in our experiments are publicly available in torchvision [36], including their official implementations, subsequent improvements, and recent training recipes that achieve state-of-the-art performance [24]. We denote these enhanced variants with “†” in this paper.

**Computing Platform.** We evaluate model performance on a single NVIDIA RTX A6000 GPU.

### 5.1 Evaluations of StableTTA-I

In our experiments, we set the batch size to 16. Since the ImageNet-1K validation set contains 50 images per class and we use a sequential sampler, the average proportion of samples belonging to the same class in a batch is 92% (see Appendix B). In Appendix H, we further discuss the results for ratios of 84% and 100%. *Since the sequential sampler can greatly improve model performance, we provide the traditional TTA results obtained with the same sequential sampler in Appendix F, Table 4, as a fair comparison to illustrate the advantage of StableTTA-I.*

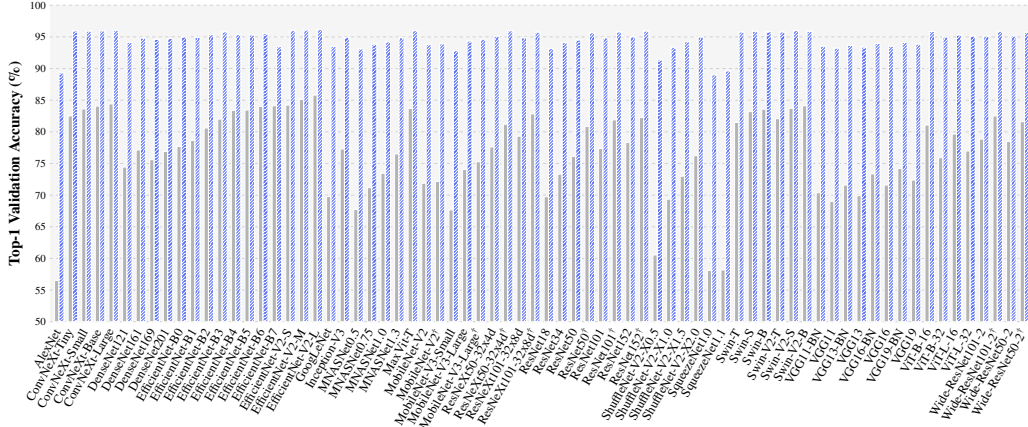


Figure 3: **Comparison under coherent-batch inference.** StableTTA-I improves model performance across a broad range of ImageNet-1K architectures under coherent-batch inference, highlighting the potential benefits of exploiting deployment-time semantic coherence during test-time aggregation.

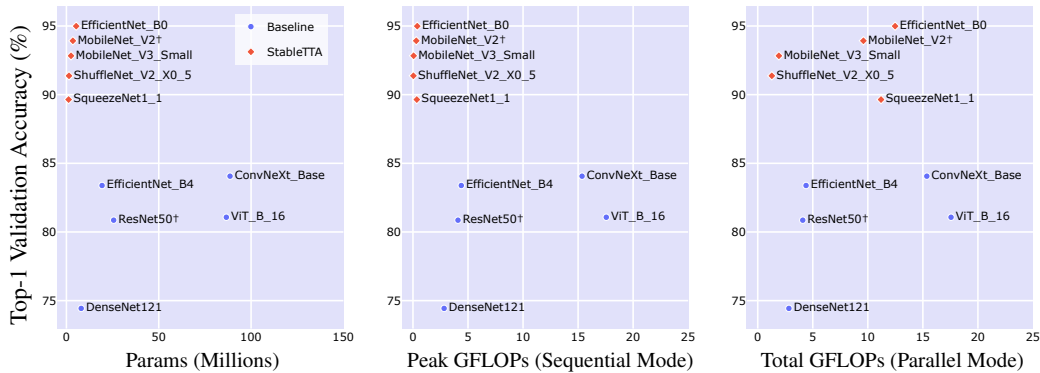


Figure 4: **Superior Efficiency and Accuracy of StableTTA-I.** Comparison of the baseline (blue) and StableTTA-I (red) across the number of model parameters (left), peak GFLOPs in sequential aggregation mode (middle), and total GFLOPs in parallel aggregation mode (right).

Fig. 3 shows that StableTTA-I consistently improves prediction accuracy across diverse ImageNet-1K models under the coherent-batch inference setting. We also report model parameter counts, computational cost, and detailed values in Appendix F (see Table 5). Fig. 4 shows that these improvements are achieved without increasing model parameters in the sequential setting of multiple forward passes, highlighting the efficiency of StableTTA-I. In the parallel setting, StableTTA-I increases inference cost by a factor of  $N$ . However, when applied to lightweight architectures, it remains significantly more economical than using large models. This demonstrates a favorable trade-off between accuracy, memory usage, and computational cost. These results suggest that StableTTA-I effectively bridges the gap between lightweight and high-performance models, enabling practical deployment in resource-constrained environments.

**Ablation Study.** We compare standard TTA using sequential sampling with our proposed StableTTA-I. As shown in Fig. 5a, StableTTA-I consistently outperforms standard TTA across different models, achieving higher top-1 and top-5 accuracy while maintaining consistent performance gains as  $N$  increases. Detailed ablation results are provided in Appendix G.

We also observed that performance gains saturate as  $N$  increases. So using a large  $N$  yields only marginal improvements. Considering the trade-off with computational cost, we adopt  $N = 32$  as a practical setting that balances performance and computational cost.

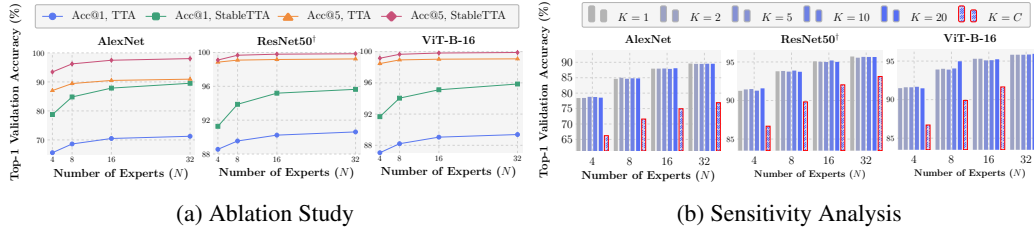


Figure 5: (a) TTA (with our sampler and augmentation) vs. StableTTA-I. (b) StableTTA-I is robust to  $K$ , but disabling logit processing ( $K = C$ ) will significantly reduce accuracy.

TTA methods employ flipping, cropping, or image translation as augmentations, resulting in improvements of classification accuracy that are modest (typically less than 2%) but require 5–100+ times additional computational cost (see Table 3 of Appendix A). In Table 4 of Appendix F and Table 6 of Appendix G, we also evaluate conventional TTA methods under the coherent-batch inference setting by adopting the same sequential sampling strategy used in StableTTA-I. Although coherent-batch inference improves the performance of all TTA methods, the gains remain smaller than those achieved by StableTTA-I. These results suggest that both the revised augmentation policy and the proposed logit processing method provide additional benefits beyond coherent-batch aggregation alone.

**Sensitivity Analysis.** We analyze the sensitivity of StableTTA-I performance with respect to its key hyperparameters, including the number of candidates  $K$  and the number of experts  $N$ . As shown in Fig. 5b, StableTTA-I demonstrates strong robustness to the choice of  $N$ , with performance remaining stable across a wide range of values. In contrast, the number of candidates  $K$  has only a marginal effect on top-1 accuracy, indicating that StableTTA-I does not strongly depend on  $K$ .

It is important to note that, when all probabilities are retained for logit averaging ( $K = C$ ), our NSS is disabled, leading to a significant performance drop and highlighting the critical role in achieving accuracy gains. These results suggest that StableTTA-I provides stable and reliable improvements without requiring meticulous hyperparameter tuning. Additional sensitivity analysis results are provided in Appendix H.

## 5.2 Evaluations of StableTTA-II

StableTTA-II is a deterministic algorithm that does not rely on sampler stochasticity, batch size, or random data augmentation. It enables improved prediction accuracy for a single image within a single forward pass. Table 2 presents the experimental results compared with the base models, demonstrating improvements across nearly all models.

The advantage of StableTTA-II lies in its simplicity and low computational cost. Using ResNet-50 as an example, its accuracy in traditional TTA mode with 10-crop augmentation reaches 77.15%, but at the cost of increasing the computational complexity of a single forward pass by 900% (see Table 3 of Appendix A). In contrast, our method improves accuracy to 77.460%, while introducing only a 0.01% computational overhead per forward pass. In Table 3 of Appendix A, we also report results from other previously published test-time augmentation methods for further comparison. Notably, these methods incur computational costs that are **multiple times higher**.

Although conceptually simple, several aspects merit further investigation. For example, our experiments show that replacing the deterministic feature-level cropping described in Section 4.2 with other values of  $k$  or random cropping leads to suboptimal results. Similarly, applying random erasing or increasing the number of “experts” degrades performance.

Furthermore, Appendix J provides a detailed description of model head configurations and feature-level cropping settings tailored to different model architectures, along with the formulation of the model head’s computation cost. In Appendix L, we further discuss possible solutions to reducing the computational cost of ensemble methods.

Table 2: Comparison of base models and the StableTTA-II-enhanced models on the ImageNet-1K.

Weight	Params	Baseline (%)		StableTTA-II (%)	
		Acc@1	Acc@5	Acc@1	Acc@5
ConvNeXt_Tiny [18, 36]	28.6M	82.520	96.146	82.570	96.218
ConvNeXt_Small [18, 36]	50.2M	83.616	96.65	83.692	96.778
ConvNeXt_Base [18, 36]	88.6M	84.062	96.87	84.208	96.952
ConvNeXt_Large [18, 36]	197.8M	84.414	96.976	84.524	97.128
DenseNet121 [10, 36]	8.0M	74.434	91.972	75.980	93.062
DenseNet161 [10, 36]	28.7M	77.138	93.56	78.586	94.366
DenseNet169 [10, 36]	14.1M	75.6	92.806	77.128	93.662
DenseNet201 [10, 36]	20.0M	76.896	93.37	78.128	94.146
EfficientNet_B0 [33, 36]	5.3M	77.692	93.532	79.074	94.408
EfficientNet_B1 [33, 36]	7.8M	78.642	94.186	79.446	94.634
EfficientNet_B2 [33, 36]	9.1M	80.608	95.31	81.014	95.454
EfficientNet_B3 [33, 36]	12.2M	82.008	96.054	82.322	96.128
EfficientNet_B4 [33, 36]	19.3M	83.384	96.594	83.060	96.306
MNASNet0_5 [35, 36]	2.2M	67.734	87.49	69.624	88.942
MNASNet0_75 [35, 36]	3.2M	71.18	90.496	71.482	90.818
MNASNet1_0 [35, 36]	4.4M	73.456	91.51	75.056	92.364
MNASNet1_3 [35, 36]	6.3M	76.506	93.522	76.720	93.736
MobileNet_V2 [27, 36]	3.5M	71.878	90.286	73.582	91.594
MobileNet_V3_Small [9, 36]	2.5M	67.668	87.402	69.570	88.774
MobileNet_V3_Large [9, 36]	5.5M	74.042	91.34	75.430	92.218
ResNeXt50_32x4d [39, 36]	25.0M	77.618	93.698	79.108	94.500
ResNeXt101_32x8d [39, 36]	88.8M	79.312	94.526	80.478	95.278
ResNeXt101_64x4d [39, 36]	88.8M	83.246	96.454	83.110	96.558
ResNet18 [7, 36]	11.7M	69.758	89.078	71.540	90.364
ResNet34 [7, 36]	21.8M	73.314	91.42	75.060	92.500
ResNet50 [7, 36]	25.6M	76.130	92.862	77.460	93.738
ResNet101 [7, 36]	44.5M	77.374	93.546	78.636	94.534
ResNet152 [7, 36]	60.2M	78.312	94.046	79.668	94.892
ShuffleNet_V2_X0_5 [21, 36]	1.4M	60.552	81.746	62.292	83.200
ShuffleNet_V2_X1_0 [21, 36]	2.3M	69.362	88.316	70.974	89.570
ShuffleNet_V2_X1_5 [21, 36]	3.5M	72.996	91.086	73.570	91.638
ShuffleNet_V2_X2_0 [21, 36]	7.4M	76.23	93.006	76.862	93.492
Wide_ResNet50_2 [41, 36]	68.9M	78.468	94.086	79.794	94.780
Wide_ResNet101_2 [41, 36]	126.9M	78.848	94.284	80.316	95.106

## 6 Limitations and Future Work

StableTTA-I assumes coherent-batch inference, where neighboring observations are semantically correlated. While this setting naturally arises in applications such as burst imaging, robotics, industrial inspection, and video perception, it does not apply to fully IID inference scenarios. Consequently, the applicability of StableTTA-I depends on deployment conditions that exhibit local semantic consistency. In addition, StableTTA-I still relies on multiple forward passes for aggregation and therefore inherits the computational overhead of conventional TTA methods. Although the method remains substantially more efficient than large-model ensembles and can be combined with lightweight architectures, reducing inference cost remains an important direction for future work. Compared with StableTTA-I, StableTTA-II provides smaller performance gains but imposes almost no practical deployment constraints. It operates with a single forward pass and negligible additional computation, although its current formulation assumes CNN-style intermediate feature tensors. For future work, we plan to extend StableTTA to other tasks, such as semantic segmentation [19] and object detection [25], and explore its integration with techniques such as model pruning [5] and knowledge distillation [8].

## 7 Conclusion

In this work, we investigate aggregation inconsistency in ensemble-based inference and show that nonlinear projection through softmax and voting operations can produce unstable predictions across aggregation strategies. We further demonstrate that this inconsistency is closely related to logit variance under coherent-batch inference settings. Motivated by this observation, we propose StableTTA-I, a training-free test-time adaptation method that improves aggregation stability through variance-aware logit processing and coherent-batch aggregation. Across diverse ImageNet-1K models, StableTTA-I produces substantial accuracy gains while maintaining favorable efficiency–performance trade-offs relative to large-model ensembles. We additionally introduce StableTTA-II, a lightweight single-forward-pass aggregation framework using feature-level cropping, enabling prediction enhancement with negligible computational overhead. Overall, our results suggest that aggregation stability provides a useful perspective for understanding and improving test-time adaptation and ensemble inference in practical visual recognition systems.

## References

- [1] Leo Breiman. Bagging predictors. *Machine learning*, 24(2):123–140, 1996.
- [2] Ekin D Cubuk, Barret Zoph, Dandelion Mane, Vijay Vasudevan, and Quoc V Le. Autoaugment: Learning augmentation strategies from data. In *Proceedings of the IEEE/CVF conference on computer vision and pattern recognition*, pages 113–123, 2019.
- [3] Jia Deng, Wei Dong, Richard Socher, Li-Jia Li, Kai Li, and Li Fei-Fei. Imagenet: A large-scale hierarchical image database. In *2009 IEEE conference on computer vision and pattern recognition*, pages 248–255. Ieee, 2009.
- [4] Alexey Dosovitskiy, Lucas Beyer, Alexander Kolesnikov, Dirk Weissenborn, Xiaohua Zhai, Thomas Unterthiner, Mostafa Dehghani, Matthias Minderer, Georg Heigold, Sylvain Gelly, et al. An image is worth 16x16 words: Transformers for image recognition at scale. *arXiv preprint arXiv:2010.11929*, 2020.
- [5] Song Han, Jeff Pool, John Tran, and William Dally. Learning both weights and connections for efficient neural network. *Advances in neural information processing systems*, 28, 2015.
- [6] Trevor Hastie. The elements of statistical learning: data mining, inference, and prediction, 2009.
- [7] Kaiming He, Xiangyu Zhang, Shaoqing Ren, and Jian Sun. Deep residual learning for image recognition. In *Proceedings of the IEEE conference on computer vision and pattern recognition*, pages 770–778, 2016.
- [8] Geoffrey Hinton, Oriol Vinyals, and Jeff Dean. Distilling the knowledge in a neural network. *arXiv preprint arXiv:1503.02531*, 2015.
- [9] Andrew Howard, Mark Sandler, Grace Chu, Liang-Chieh Chen, Bo Chen, Mingxing Tan, Weijun Wang, Yukun Zhu, Ruoming Pang, Vijay Vasudevan, et al. Searching for mobilenetv3. In *Proceedings of the IEEE/CVF international conference on computer vision*, pages 1314–1324, 2019.
- [10] Gao Huang, Zhuang Liu, Laurens Van Der Maaten, and Kilian Q Weinberger. Densely connected convolutional networks. In *Proceedings of the IEEE conference on computer vision and pattern recognition*, pages 4700–4708, 2017.
- [11] Forrest N Iandola, Song Han, Matthew W Moskewicz, Khalid Ashraf, William J Dally, and Kurt Keutzer. Squeezenet: Alexnet-level accuracy with 50x fewer parameters and < 0.5 mb model size. *arXiv preprint arXiv:1602.07360*, 2016.
- [12] Carlos M Jarque and Anil K Bera. Efficient tests for normality, homoscedasticity and serial independence of regression residuals. *Economics letters*, 6(3):255–259, 1980.
- [13] Ildoo Kim, Younghoon Kim, and Sungwoong Kim. Learning loss for test-time augmentation. *Advances in neural information processing systems*, 33:4163–4174, 2020.

- [14] Alex Krizhevsky, Ilya Sutskever, and Geoffrey E Hinton. Imagenet classification with deep convolutional neural networks. *Advances in neural information processing systems*, 25, 2012.
- [15] Zheng Li, Jerry Cheng, and Huanying Helen Gu. Losstransform: Reformulating the loss function for contrastive learning. *Information*, 16(12):1068, 2025.
- [16] Ze Liu, Yutong Lin, Yue Cao, Han Hu, Yixuan Wei, Zheng Zhang, Stephen Lin, and Baining Guo. Swin transformer: Hierarchical vision transformer using shifted windows. In *Proceedings of the IEEE/CVF international conference on computer vision*, pages 10012–10022, 2021.
- [17] Ze Liu, Han Hu, Yutong Lin, Zhuliang Yao, Zhenda Xie, Yixuan Wei, Jia Ning, Yue Cao, Zheng Zhang, Li Dong, et al. Swin transformer v2: Scaling up capacity and resolution. In *Proceedings of the IEEE/CVF conference on computer vision and pattern recognition*, pages 12009–12019, 2022.
- [18] Zhuang Liu, Hanzi Mao, Chao-Yuan Wu, Christoph Feichtenhofer, Trevor Darrell, and Saining Xie. A convnet for the 2020s. In *Proceedings of the IEEE/CVF conference on computer vision and pattern recognition*, pages 11976–11986, 2022.
- [19] Jonathan Long, Evan Shelhamer, and Trevor Darrell. Fully convolutional networks for semantic segmentation. In *Proceedings of the IEEE conference on computer vision and pattern recognition*, pages 3431–3440, 2015.
- [20] Alexander Lyzhov, Yuliya Molchanova, Arsenii Ashukha, Dmitry Molchanov, and Dmitry Vetrov. Greedy policy search: A simple baseline for learnable test-time augmentation. In *Conference on uncertainty in artificial intelligence*, pages 1308–1317. PMLR, 2020.
- [21] Ningning Ma, Xiangyu Zhang, Hai-Tao Zheng, and Jian Sun. Shufflenet v2: Practical guidelines for efficient cnn architecture design. In *Proceedings of the European conference on computer vision (ECCV)*, pages 116–131, 2018.
- [22] Dhruv Mahajan, Ross Girshick, Vignesh Ramanathan, Kaiming He, Manohar Paluri, Yixuan Li, Ashwin Bharambe, and Laurens Van Der Maaten. Exploring the limits of weakly supervised pretraining. In *Proceedings of the European conference on computer vision (ECCV)*, pages 181–196, 2018.
- [23] Fabian Pedregosa, Gaël Varoquaux, Alexandre Gramfort, Vincent Michel, Bertrand Thirion, Olivier Grisel, Mathieu Blondel, Peter Prettenhofer, Ron Weiss, Vincent Dubourg, et al. Scikit-learn: Machine learning in python. *the Journal of machine Learning research*, 12:2825–2830, 2011.
- [24] PyTorch Team. How to train state-of-the-art models using torchvision’s latest primitives. <https://pytorch.org/blog/how-to-train-state-of-the-art-models-using-torchvision-latest-primitives/>, 2021. Accessed: 2026-03-25.
- [25] Shaoqing Ren, Kaiming He, Ross Girshick, and Jian Sun. Faster r-cnn: Towards real-time object detection with region proposal networks. *Advances in neural information processing systems*, 28, 2015.
- [26] Tal Ridnik, Emanuel Ben-Baruch, Asaf Noy, and Lihi Zelnik-Manor. Imagenet-21k pretraining for the masses. *arXiv preprint arXiv:2104.10972*, 2021.
- [27] Mark Sandler, Andrew Howard, Menglong Zhu, Andrey Zhmoginov, and Liang-Chieh Chen. Mobilenetv2: Inverted residuals and linear bottlenecks. In *Proceedings of the IEEE conference on computer vision and pattern recognition*, pages 4510–4520, 2018.
- [28] Divya Shanmugam, Davis Blalock, Guha Balakrishnan, and John Guttag. Better aggregation in test-time augmentation. In *Proceedings of the IEEE/CVF international conference on computer vision*, pages 1214–1223, 2021.
- [29] Divya Shanmugam, Helen Lu, Swami Sankaranarayanan, and John Guttag. Test-time augmentation improves efficiency in conformal prediction. In *Proceedings of the Computer Vision and Pattern Recognition Conference*, pages 20622–20631, 2025.

- [30] Karen Simonyan and Andrew Zisserman. Very deep convolutional networks for large-scale image recognition. *arXiv preprint arXiv:1409.1556*, 2014.
- [31] Christian Szegedy, Wei Liu, Yangqing Jia, Pierre Sermanet, Scott Reed, Dragomir Anguelov, Dumitru Erhan, Vincent Vanhoucke, and Andrew Rabinovich. Going deeper with convolutions. In *Proceedings of the IEEE conference on computer vision and pattern recognition*, pages 1–9, 2015.
- [32] Christian Szegedy, Vincent Vanhoucke, Sergey Ioffe, Jon Shlens, and Zbigniew Wojna. Rethinking the inception architecture for computer vision. In *Proceedings of the IEEE conference on computer vision and pattern recognition*, pages 2818–2826, 2016.
- [33] Mingxing Tan and Quoc Le. Efficientnet: Rethinking model scaling for convolutional neural networks. In *International conference on machine learning*, pages 6105–6114. PMLR, 2019.
- [34] Mingxing Tan and Quoc Le. Efficientnetv2: Smaller models and faster training. In *International conference on machine learning*, pages 10096–10106. PMLR, 2021.
- [35] Mingxing Tan, Bo Chen, Ruoming Pang, Vijay Vasudevan, Mark Sandler, Andrew Howard, and Quoc V Le. Mnasnet: Platform-aware neural architecture search for mobile. In *Proceedings of the IEEE/CVF conference on computer vision and pattern recognition*, pages 2820–2828, 2019.
- [36] TorchVision Contributors. Torchvision: Pytorch’s computer vision library, 2016. <https://github.com/pytorch/vision>.
- [37] Zhengzhong Tu, Hossein Talebi, Han Zhang, Feng Yang, Peyman Milanfar, Alan Bovik, and Yinxiao Li. Maxvit: Multi-axis vision transformer. In *European conference on computer vision*, pages 459–479. Springer, 2022.
- [38] Aladin Virmaux and Kevin Scaman. Lipschitz regularity of deep neural networks: analysis and efficient estimation. *Advances in neural information processing systems*, 31, 2018.
- [39] Saining Xie, Ross Girshick, Piotr Dollár, Zhuowen Tu, and Kaiming He. Aggregated residual transformations for deep neural networks. In *Proceedings of the IEEE conference on computer vision and pattern recognition*, pages 1492–1500, 2017.
- [40] Sangdoon Yun, Dongyoon Han, Seong Joon Oh, Sanghyuk Chun, Junsuk Choe, and Youngjoon Yoo. Cutmix: Regularization strategy to train strong classifiers with localizable features. In *Proceedings of the IEEE/CVF international conference on computer vision*, pages 6023–6032, 2019.
- [41] Sergey Zagoruyko and Nikos Komodakis. Wide residual networks. *arXiv preprint arXiv:1605.07146*, 2016.
- [42] Hongyi Zhang, Moustapha Cisse, Yann N Dauphin, and David Lopez-Paz. mixup: Beyond empirical risk minimization. In *International Conference on Learning Representations*, 2018.

## A Preliminary Concepts and Reproduction of Prior Work

In this section, we review key concepts and reproduce prior TTA results to highlight their limitations and motivate our method.

Fig. 6 illustrates three common inference strategies for model predictions. (a) shows the baseline approach, where a single model processes the input once to produce an output. (b) presents a multi-model ensemble, in which predictions from several independently trained models are combined to improve accuracy, at the cost of increasing the total model size and the computational overhead. (c) demonstrates TTA, where multiple augmented images of the same input are passed through a single model and their predictions are aggregated. While both ensemble methods (b) and (c) can enhance performance compared to the baseline (a), they require multiple forward passes, leading to higher inference cost.

In addition, Table 3 summarizes representative TTA results reported on the ImageNet-1K validation set. A range of augmentation policies, such as AutoAugment, flipping, cropping, and GPS, have been

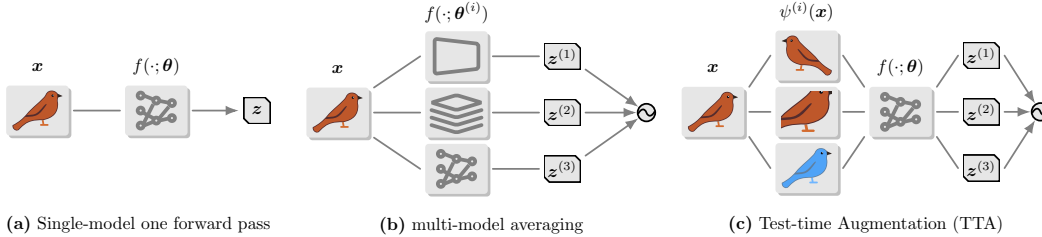


Figure 6: (a) **Baseline**: a single model with one forward pass. (b) **Multi-model ensemble**: multiple models with multiple forward passes. (c) **TTA**: a single model with multiple forward passes using augmented inputs. Both the multi-model ensemble and TTA aggregate outputs across forward passes.

evaluated across diverse architectures. Although these methods consistently improve accuracy over baseline (single-pass inference), the gains remain limited: all reported results stay below 80% top-1 accuracy, incurring increased inference cost due to multiple forward passes.

Table 3: Summary of experimental results reported in prior studies, evaluated using top-1 accuracy on the ImageNet-1K validation set. Both baseline and test-time augmentation (TTA) results are taken directly from the original papers, with each value corresponding to its respective reference.

Weight	Data Augmentation	Baseline	TTA Acc	Source paper
VGG(v5)	10 × Crop		71.93	[7] He et al.
PReLU-net	10 × Crop		75.73	[7] He et al.
plain-34	10 × Crop		71.46	[7] He et al.
ResNet50	10 × Crop		77.15	[7] He et al.
ResNet101	10 × Crop		78.25	[7] He et al.
ResNet152	10 × Crop		78.57	[7] He et al.
DenseNet-121	10 × Crop	74.98	76.39	[10] Huang et al.
DenseNet-169	10 × Crop	76.20	77.92	[10] Huang et al.
DenseNet-201	10 × Crop	77.42	78.54	[10] Huang et al.
DenseNet-264	10 × Crop	77.85	79.20	[10] Huang et al.
MobileNetV2	30 × AutoAugment		71.38	[28] Shanmugam et al.
InceptionV3	30 × AutoAugment		69.51	[28] Shanmugam et al.
ResNet18	30 × AutoAugment		69.62	[28] Shanmugam et al.
ResNet50	30 × AutoAugment		75.53	[28] Shanmugam et al.
MobileNetV2	128 × (AutoAugment+[28])		72.57	[28] Shanmugam et al.
InceptionV3	128 × (AutoAugment+[28])		71.02	[28] Shanmugam et al.
ResNet18	128 × (AutoAugment+[28])		70.89	[28] Shanmugam et al.
ResNet50	128 × (AutoAugment+[28])		76.36	[28] Shanmugam et al.
ResNet50	5 × Crop		76.19	[13] Kim et al.
ResNet50	10 × Crop		76.94	[13] Kim et al.
ResNet50	4 × GPS [20]		76.56	[13] Kim et al.
ResNet50	2 × Flip + 2 × [13]		77.90	[13] Kim et al.
ResNet50	5 × Crop + 2 × [13]		79.34	[13] Kim et al.

## B Sequential Sampling and Data Augmentation Policies of StatbleTTA-I

**Sequential Sampling.** The ImageNet-1K validation set contains 50,000 images, organized into 1,000 classes with 50 images per class, stored sequentially by class. When sampling this dataset sequentially using a small batch size (without shuffling), batches are not class-balanced: most batches contain samples predominantly from a single class, with occasional boundary batches that mix two adjacent classes. For example, when the batch size is set to 16, the dataset is partitioned into groups of image-label pairs as follows:

$$\underbrace{(\text{img}_1, C_1), \dots, (\text{img}_{17}, C_1)}_{\text{1st batch}}, \underbrace{(\text{img}_{17}, C_1), \dots, (\text{img}_{33}, C_1)}_{\text{2nd batch}}, \underbrace{(\text{img}_{33}, C_1), \dots, (\text{img}_{49}, C_1)}_{\text{3rd batch}}, \underbrace{(\text{img}_{49}, C_1), \dots, (\text{img}_{64}, C_2)}_{\text{4th batch}}, \dots$$

Since batch boundaries and class boundaries repeat every

$$\text{lcm}(50, 16) = 400,$$

each cycle contains  $400/16 = 25$  batches. Within each cycle, the number of samples from the majority class in each batch follows the pattern:

16, 16, 16, 14, 16, 16, 12, 16, 16, 10, 16, 16, 8, 16, 16, 10, 16, 16, 12, 16, 16, 14, 16, 16, 16.

The average majority-class ratio is  $368/400 = 92\%$ .

**Augmentation Policies.** Since neural network layers are continuous and differentiable, most neural networks satisfy the Hölder condition [38]:

$$\|z - z'\| = \|f(\mathbf{x}; \boldsymbol{\theta}) - f(\mathbf{x}'; \boldsymbol{\theta})\| \leq c \cdot \|\mathbf{x} - \mathbf{x}'\|^d,$$

where  $c$  and  $d$  are some constants. This inequality indicates that the distance  $\|z - z'\|$  between logits is bounded by the distance  $\|\mathbf{x} - \mathbf{x}'\|$  between inputs.

Now, consider a sequence of data augmentations  $\{\psi_1, \psi_2, \dots\}$  and the corresponding logit vector  $\mathbf{z}^{(i)} := f(\psi_i(\mathbf{x}); \boldsymbol{\theta})$ . By applying the Hölder condition, we obtain:

$$\|\mathbf{z}^{(i)} - \mathbf{z}^{(j)}\| = \|f(\psi_i(\mathbf{x}); \boldsymbol{\theta}) - f(\psi_j(\mathbf{x}); \boldsymbol{\theta})\| \leq c \cdot \|\psi_i(\mathbf{x}) - \psi_j(\mathbf{x})\|^d. \quad (2)$$

To facilitate understanding Eq. (2), in Appendix E, we provide Fig. 9 for visualization, along with empirical results as supporting evidence.

When  $d \in (0, 1]$ , since  $\mathbf{z}, \mathbf{z}'$  are independent and identically distributed, and using the identity  $\mathbb{E}\|\mathbf{z} - \mathbf{z}'\|^2 = 2 \text{Var}(\mathbf{z})$ , Jensen’s inequality gives:

$$\text{Var}(\mathbf{z}) \leq 2^{d-1} c^2 \text{Var}(\psi(\mathbf{x})).$$

Now, revisiting the inconsistency discussed in Section 3, we evaluate data augmentation policies as follows: (1) Simple augmentation methods such as horizontal flipping and random cropping are not necessary in TTA, as the model is not sensitive to them (see Table 4 of Appendix F). These techniques are standard in model training and provide only marginal improvements. Consequently, the resulting logit vectors are typically identical after such augmentations. (2) Strong augmentation techniques such as translation, rotation, and affine transformations [2] should be avoided in TTA, as they can induce an excessively large increase in  $\text{Var}(\psi(\mathbf{x}))$ . (3) Although random erasing yields relatively small values of  $\text{Var}(\psi(\mathbf{x}))$ , it provides limited diversity among augmented samples and is therefore excluded. (4) Mixup [42] and CutMix [40] are strong data augmentation methods; however, they operate across image patches, which may alter the ground-truth labels. Therefore, when applying mixup or CutMix, we need to ensure that the batch of images largely belongs to the same class.

Under these considerations, mixup and CutMix emerge as promising candidates. However, both require further modification to reduce  $\text{Var}(\psi(\mathbf{x}))$ :

- **Mixup:** Instead of combining the input with a random image, we perform a weighted combination with a fixed image, which is randomly sampled and kept unchanged thereafter.
- **CutMix:** The covering region is typically sampled from a Beta distribution to encourage diversity during training. In contrast, we fix the window size to one-quarter of the image to reduce  $\text{Var}(\psi(\mathbf{x}))$ .
- **Random Choice:** Standard pipelines often compose multiple augmentations. Here, we randomly choose mixup or CutMix in each forward pass to better control  $\text{Var}(\psi(\mathbf{x}))$ .

## C Jarque–Bera Test of StableTTA-I

To support the assumption we used in Section 4.1, we introduce the Jarque–Bera test [12] and then empirically show that the logit  $z_k \sim \mathcal{N}(\boldsymbol{\mu}_k, \sigma_k^2)$ , based on our proposed data augmentation policies for any  $k \in \{1, \dots, C\}$ . We select the Jarque–Bera test, which is suitable for small sample sizes, with  $N \leq 32$  in our setting.

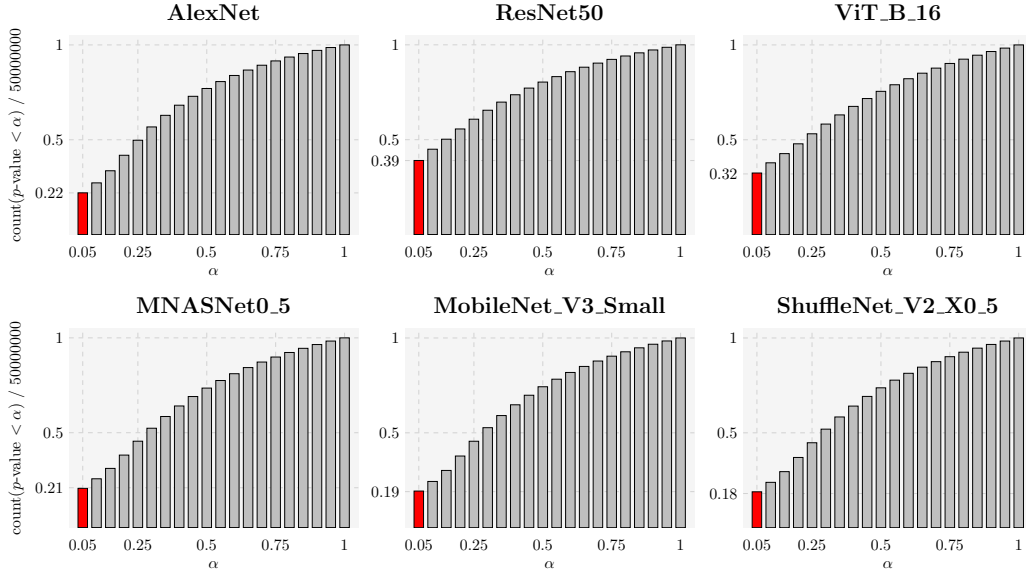


Figure 7: Empirical cumulative distribution functions (ECDFs) of  $p$ -values from Jarque–Bera tests across models on ImageNet-1K validation set. Each model outputs  $50,000 \times 1,000$  groups from augmented images, with one test per group. The x-axis shows the significance level  $\alpha$ , and the y-axis shows the proportion of  $p$ -values  $\leq \alpha$ . The red bar marks the case of  $\alpha = 0.05$ . A lower proportion (e.g., 22% of the tested groups under AlexNet) indicates that the majority of groups fail to reject the null hypothesis, suggesting stronger consistency with a normal distribution.

For a given  $k \in \{1, \dots, C\}$ , we consider the hypothesis:

$$H_0 : z_k^{(1)}, \dots, z_k^{(N)} \stackrel{\text{i.i.d.}}{\sim} \mathcal{N}(\mu_k, \sigma_k^2),$$

where  $\mu_k \in \mathbb{R}$  and  $\sigma_k > 0$  are unknown parameters. In Jarque–Bera test, under  $H_0$ :

$$JB = \frac{N}{6} \left( S^2 + \frac{(K - 3)^2}{4} \right) \stackrel{\text{approx.}}{\sim} \chi^2(2),$$

where  $S$  is the skewness and  $K$  is the kurtosis. Therefore, at significance level  $\alpha = 0.05$ , we reject  $H_0$  if:

$$JB > \chi_{0.95,2}^2 \approx 5.99.$$

Based on this, we design a Monte Carlo test to verify the hypothesis. Since the ImageNet-1K validation set contains 50,000 images across 1,000 classes, we obtain  $50,000 \times 1,000$  groups, each of which consists of  $N$  individual data points  $\{z_k^{(1)}, \dots, z_k^{(N)}\}$ . For each group, a Jarque–Bera test is conducted to evaluate the  $H_0$  that the samples follow a normal distribution. To better understanding, we perform  $N$  individual data augmentations on the 50,000 images. The AlexNet model then outputs  $N \times 50,000$  logit vectors with the dimension of 1,000. Thus, we obtain  $50,000 \times 1,000$  groups (each with  $N$  samples), and our goal is to test whether each group follows a normal distribution. Consequently, for each model shown in Fig. 7, we plot the empirical cumulative distribution function (cumulating histogram) of the resulting 50,000,000  $p$ -values, where the x-axis represents significance levels ( $\alpha$ ) ranging from 0 to 1, and the y-axis shows the cumulative proportion of tests with  $p$ -values less than or equal to each  $\alpha$ . These histograms present an overall assessment of how often the normality assumption holds across all images and classes.

The figure shows that, in AlexNet’s outputs, 22% of the groups have  $p$ -values less than 0.05. This implies that 78% of the groups fail to reject the null hypothesis  $H_0$ , suggesting that these groups are consistent with a normal distribution. Similar trends are observed for other models.

## D Monte Carlo Simulation of StableTTA-I

In this section, we present a Monte Carlo simulation with mathematical derivations and experimental visualizations to support our explanation of the aggregation inconsistency phenomenon introduced in Section 3.

Based on our discussion in Appendix C, we assume that the logit vector  $\mathbf{z} \sim \mathcal{N}(\boldsymbol{\mu}, \sigma^2 \mathbf{I})$  in a binary classification task. Then,

$$\mathbb{E} \begin{pmatrix} z_1 - z_2 \\ \mathbb{1}_{z_1 > z_2} \end{pmatrix} = \begin{bmatrix} \boldsymbol{\mu}_1 - \boldsymbol{\mu}_2 \\ \Phi \left( \frac{\boldsymbol{\mu}_1 - \boldsymbol{\mu}_2}{\sqrt{2}\sigma} \right) \end{bmatrix}, \quad (3)$$

$$\text{Var} \begin{pmatrix} z_1 - z_2 \\ \mathbb{1}_{z_1 > z_2} \end{pmatrix} = \begin{bmatrix} 2\sigma^2 & \sqrt{2}\sigma\phi(a) \\ \sqrt{2}\sigma\phi(a) & \Phi(a) - \Phi^2(a) \end{bmatrix}, \quad (4)$$

where

$$a = \frac{\boldsymbol{\mu}_1 - \boldsymbol{\mu}_2}{\sqrt{2}\sigma}.$$

By the Central Limit Theorem, for large  $N$ , the sample averages satisfy

$$\begin{pmatrix} \frac{1}{N} \sum_{i=1}^N z_1^{(i)} - z_2^{(i)} \\ \frac{1}{N} \sum_{i=1}^N \mathbb{1}_{z_1^{(i)} > z_2^{(i)}} \end{pmatrix} \sim \mathcal{N} \left( \begin{bmatrix} \boldsymbol{\mu}_1 - \boldsymbol{\mu}_2 \\ \Phi \left( \frac{\boldsymbol{\mu}_1 - \boldsymbol{\mu}_2}{\sqrt{2}\sigma} \right) \end{bmatrix}, \frac{1}{N} \begin{bmatrix} 2\sigma^2 & \sqrt{2}\sigma\phi(a) \\ \sqrt{2}\sigma\phi(a) & \Phi(a) - \Phi^2(a) \end{bmatrix} \right).$$

Define the standardized variables

$$\begin{bmatrix} X \\ Y \end{bmatrix} := \begin{bmatrix} \frac{\frac{1}{N} \sum_{i=1}^N (z_1^{(i)} - z_2^{(i)}) - (\boldsymbol{\mu}_1 - \boldsymbol{\mu}_2)}{\sqrt{2}\sigma/\sqrt{N}} \\ \frac{\frac{1}{N} \sum_{i=1}^N \mathbb{1}_{z_1^{(i)} > z_2^{(i)}} - \Phi(a)}{\sqrt{\Phi(a) - \Phi^2(a)}/\sqrt{N}} \end{bmatrix},$$

which jointly follow

$$\begin{bmatrix} X \\ Y \end{bmatrix} \sim \mathcal{N} \left( \begin{bmatrix} 0 \\ 0 \end{bmatrix}, \begin{bmatrix} 1 & \frac{\phi(a)}{\sqrt{\Phi(a)(1-\Phi(a))}} \\ \frac{\phi(a)}{\sqrt{\Phi(a)(1-\Phi(a))}} & 1 \end{bmatrix} \right).$$

We now compute the probability of aggregation inconsistency between the logit-averaging and the hard voting method. First,

$$\begin{aligned} \mathbb{P}(\hat{y}_{\text{logit}} = 1, \hat{y}_{\text{hard}} = 2) &= \mathbb{P} \left( \frac{1}{N} \sum_{k=1}^N (z_1^{(k)} - z_2^{(k)}) > 0, \frac{1}{N} \sum_{i=1}^N \mathbb{1}_{z_1^{(i)} > z_2^{(i)}} \leq \frac{1}{2} \right) \\ &= \mathbb{P} \left( X > -\sqrt{N}a, Y \leq \frac{(1/2 - \phi(a))\sqrt{N}}{\sqrt{\Phi(a) - \Phi^2(a)}} \right) \\ &= \Phi \left( \frac{(1/2 - \Phi(a))\sqrt{N}}{\sqrt{\Phi(a) - \Phi^2(a)}} \right) \\ &\quad - \Phi_2 \left( -a\sqrt{N}, \frac{(1/2 - \Phi(a))\sqrt{N}}{\sqrt{\Phi(a) - \Phi^2(a)}}; \frac{\phi(a)}{\sqrt{\Phi(a) - \Phi^2(a)}} \right), \end{aligned} \quad (5)$$

where  $\Phi$  and  $\Phi_2$  denote the cumulative distribution function (CDF) of the standard normal distribution and the joint CDF of the standard bivariate normal distribution, respectively.

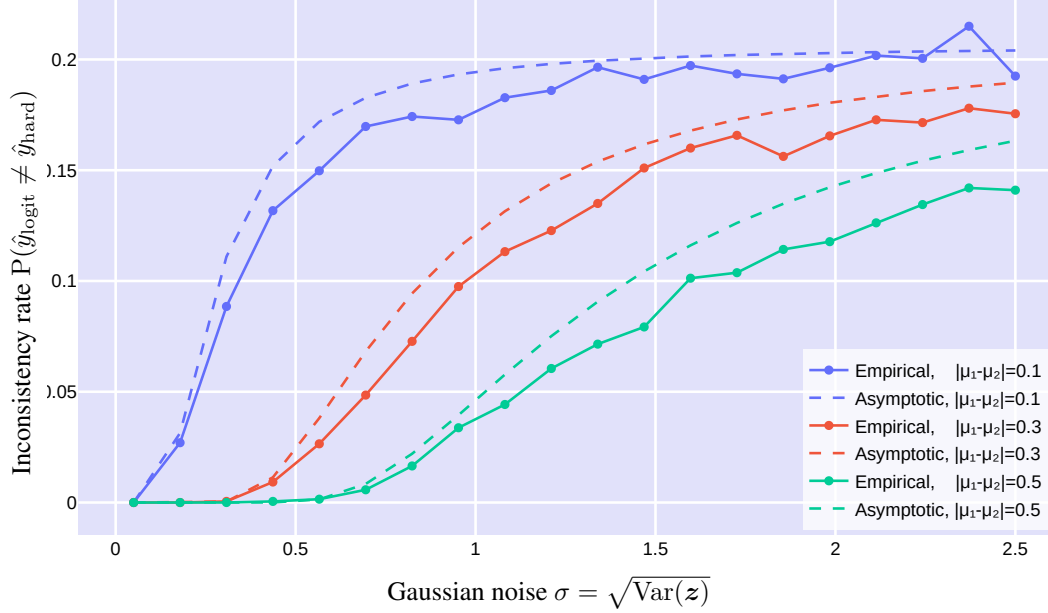


Figure 8: **Monte Carlo simulation.** The inconsistency probability increases as  $\text{Var}(z)$  grows. In this simulation, we consider distributions:  $\{z \sim \mathcal{N}(\mu, \sigma I) \mid \mu \in \{(1, 0.9), (1, 0.7), (1, 0.5)\}, \sigma \in [0.05, 0.25]\}$ . The solid curves show Monte Carlo estimates of the relationship between  $\sigma$  and  $P(\hat{y}_{\text{logit}} \neq \hat{y}_{\text{hard}})$ , while the dashed curves correspond to the theoretical (asymptotic) predictions. The empirical and theoretical results are closely matched.

Similarly,

$$\begin{aligned}
P(\hat{y}_{\text{logit}} = 2, \hat{y}_{\text{hard}} = 1) &= P\left(\frac{1}{N} \sum_{k=1}^N (z_1^{(k)} - z_2^{(k)}) \leq 0, \frac{1}{N} \sum_{i=1}^N \mathbb{1}_{z_1^{(k)} > z_2^{(k)}} > \frac{1}{2}\right) \\
&= P\left(X \leq -\sqrt{N}a, Y > \frac{(1/2 - \phi(a))\sqrt{N}}{\sqrt{\Phi(a) - \Phi^2(a)}}\right) \\
&= \Phi(-\sqrt{N}a) \\
&\quad - \Phi_2\left(-a\sqrt{N}, \frac{(1/2 - \Phi(a))\sqrt{N}}{\sqrt{\Phi(a) - \Phi^2(a)}}; \frac{\phi(a)}{\sqrt{\Phi(a) - \Phi^2(a)}}\right). \tag{6}
\end{aligned}$$

Therefore, the total inconsistency probability is

$$\begin{aligned}
P(\hat{y}_{\text{logit}} \neq \hat{y}_{\text{hard}}) &= P(\hat{y}_{\text{logit}} = 1, \hat{y}_{\text{hard}} = 2) + P(\hat{y}_{\text{logit}} = 2, \hat{y}_{\text{hard}} = 1) \\
&= \Phi(-\sqrt{N}a) + \Phi\left(\frac{(1/2 - \Phi(a))\sqrt{N}}{\sqrt{\Phi(a) - \Phi^2(a)}}\right) \\
&\quad - 2\Phi_2\left(-a\sqrt{N}, \frac{(1/2 - \Phi(a))\sqrt{N}}{\sqrt{\Phi(a) - \Phi^2(a)}}; \frac{\phi(a)}{\sqrt{\Phi(a) - \Phi^2(a)}}\right). \tag{7}
\end{aligned}$$

This expression indicates that the inconsistency rate increases as  $\text{Var}(z) = \sigma^2$  grows. Fig. 8 provides empirical support for this conclusion. The solid curves represent Monte Carlo estimates of the relationship between  $\sigma$  and  $P(\hat{y}_{\text{logit}} \neq \hat{y}_{\text{hard}})$ , while the dashed curves correspond to the theoretical (asymptotic) predictions. We observe that the empirical and theoretical curves closely match.

## E Hölder Condition of StableTTA-I

In this section, we present a visualization to explain the Hölder condition introduced in Eq. (2).

Figure 9 provides an intuitive visualization of how different data augmentation strategies influence the variance of logits under the Hölder continuity assumption. According to Eq. (2), the distance between logit vectors is bounded by the distance between augmented inputs. As illustrated in the left example, translation preserves the semantic structure of the image but introduces large pixel-wise differences between augmented samples, leading to a larger input distance  $|\psi_i(\mathbf{x}) - \psi_j(\mathbf{x})|$  and consequently higher variance in the resulting logits. In contrast, the right example shows random erasing, which applies stronger augmentations but gives smaller overall pixel-wise differences. This reduces the variance of the logit vector, producing more concentrated predictions that are better suited for stable aggregation. The figure thus highlights that not all augmentations contribute equally to logit stability. Our proposed augmentation policies (Var = 0.12) exhibit higher variance than random horizontal flipping (Var = 0.005) and random cropping (Var = 0.01), but significantly lower than the composition of raw MixUp and CutMix (Var = 0.16).

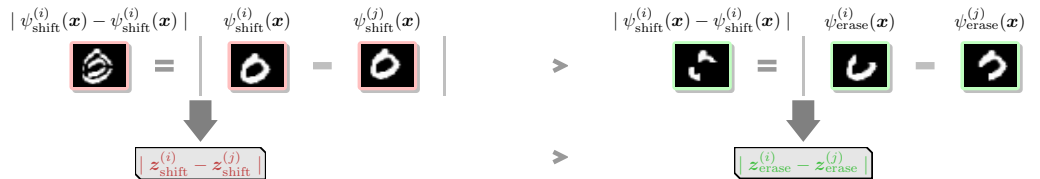


Figure 9: **Varying Effects of Data Augmentation Methods on the Variance of Logits.** Under Hölder continuity, larger changes in the input lead to larger changes in the logits. **Left:** Translation preserves the semantic content of the image but introduces large pixel-wise differences, resulting in a higher variations in the logits. **Right:** Random erasing applies stronger modifications to the image, but the overall pixel-wise differences are smaller, leading to more concentrated logits that are better suited to stable aggregation.

## F Comparison Experiments of StableTTA-I

Although existing studies primarily rely on simple augmentation policies such as flipping and cropping, we consider the sequential sampling and explore a broader range of strategies to better understand their impact on standard TTA performance and provide a more comprehensive evaluation. In Table 4, we conduct experiments on both large and small models, including AlexNet, ResNet (with current best recipes), and ViT\_B\_16 with diverse  $N$ , as well as MNASNet0\_5, MobileNetV3-Small, and ShuffleNetV2\_x0\_5. All pretrained models are obtained from TorchVision. The results show that logit averaging slightly outperforms both hard and soft voting aggregation strategies. We adopt standard data augmentation policies with TorchVision default hyperparameters, including horizontal flip ( $p = 0.5$ ), random crop (padding=32), random affine transformations (maximum rotation=15°, translation=(0.1, 0.1), scale range=(0.9, 1.1), shear=10), random erasing ( $p=0.1$ ), mixup ( $\alpha = 0.2$ ), and CutMix ( $\alpha = 1.0$ ).

Table 4: Comparison of aggregation strategies (hard voting, soft voting, and logit averaging) under random data augmentation across different models. All results are derived from our aforementioned experiments using TorchVision pretrained models.

Model	Random Data Augmentation	Hard-vot. (%)		Soft-vot. (%)		Logit-avg. (%)	
		Acc@1	Acc@5	Acc@1	Acc@5	Acc@1	Acc@5
AlexNet (# Params = 61.1 M) (7.1 GFLOPS) ( $N = 10$ )	baseline	56.522	79.066	56.522	79.066	56.522	79.066
	flip	56.630	56.760	57.306	79.674	57.322	79.714
	crop	55.016	55.158	55.460	78.240	55.002	78.082
	affine	51.176	51.342	51.966	75.262	51.116	74.564
	erasing	56.552	56.688	56.574	78.914	56.508	79.070

*Continued on next page*

Model	Augmentation	Acc@1	Acc@5	Acc@1	Acc@5	Acc@1	Acc@5
	mixup	59.374	59.506	68.178	89.594	73.578	91.156
	CutMix	63.356	63.460	65.754	87.124	66.814	87.172
	flip+crop	55.292	55.434	55.850	78.376	55.606	78.278
	mixup+CutMix	64.320	64.420	69.552	89.904	72.466	90.802
ResNet50 <sup>†</sup> (# Params = 25.6 M) (40.9 GFLOPS) ( $N = 10$ )	baseline	80.858	95.434	80.858	95.434	80.858	95.434
	flip	80.740	80.774	81.048	95.586	81.040	95.572
	crop	80.896	80.932	80.984	95.590	80.946	95.542
	affine	76.304	76.380	76.886	93.464	76.664	93.174
	erasing	80.844	80.878	80.828	95.428	80.804	95.442
	mixup	82.904	82.936	87.380	98.958	89.284	98.806
	CutMix	89.550	89.574	90.610	99.182	90.466	99.154
	flip+crop	81.050	81.090	81.152	95.616	81.070	95.588
mixup+CutMix	87.906	87.930	89.812	99.134	90.338	99.172	
ViT_B_16 (# Params = 86.6 M) (175.6 GFLOPS) ( $N = 10$ )	baseline	81.072	95.318	81.072	95.318	81.072	95.318
	flip	81.034	81.086	81.024	95.302	81.024	95.318
	crop	81.258	81.300	81.422	95.556	81.188	95.526
	affine	80.134	80.186	80.250	94.880	80.116	94.904
	erasing	81.070	81.120	81.048	95.280	81.060	95.306
	mixup	83.258	83.300	86.998	98.858	89.508	98.910
	CutMix	87.392	87.420	88.132	98.748	88.622	98.778
	flip+crop	81.338	81.386	81.280	95.550	81.218	95.482
mixup+CutMix	86.840	86.868	88.504	98.936	89.798	99.080	
AlexNet (# Params = 61.1 M) (22.75 GFLOPS) ( $N = 32$ )	baseline	56.522	79.066	56.522	79.066	56.522	79.066
	flip	56.520	56.652	57.322	79.722	57.404	79.736
	crop	55.530	55.672	55.734	78.444	55.458	78.194
	affine	52.142	52.296	52.654	75.716	51.632	75.162
	erasing	56.552	56.688	56.540	79.036	56.550	79.094
	mixup	61.918	62.022	69.878	90.004	75.500	92.426
	CutMix	65.854	65.960	67.672	88.374	68.062	88.122
	flip+crop	55.950	56.096	56.316	78.728	55.840	78.526
mixup+CutMix	67.166	67.252	71.296	90.930	74.522	91.972	
ResNet50 <sup>†</sup> (# Params = 25.6 M) (130.9 GFLOPS) ( $N = 32$ )	baseline	80.858	95.434	80.858	95.434	80.858	95.434
	flip	80.842	80.874	81.012	95.598	81.072	95.578
	crop	81.058	81.098	81.122	95.626	81.072	95.582
	affine	76.762	76.844	77.222	93.542	76.818	93.342
	erasing	80.844	80.878	80.832	95.414	80.838	95.406
	mixup	84.286	84.318	88.212	99.038	90.472	99.186
	CutMix	90.394	90.410	90.964	99.248	90.770	99.228
	flip+crop	81.236	81.274	81.186	95.654	81.196	95.600
mixup+CutMix	89.702	89.718	90.602	99.216	91.296	99.308	
ViT_B_16 (# Params = 86.6 M) (561.9 GFLOPS) ( $N = 32$ )	baseline	81.072	95.318	81.072	95.318	81.072	95.318
	flip	81.004	81.054	81.022	95.300	81.006	95.300
	crop	81.430	81.472	81.428	95.598	81.376	95.588
	affine	80.316	80.368	80.394	95.018	80.288	95.014
	erasing	81.068	81.118	81.066	95.276	81.064	95.302
	mixup	84.976	84.914	88.176	98.966	90.566	99.292
	CutMix	87.996	88.024	88.574	98.930	89.040	98.912
	flip+crop	81.346	81.388	81.448	95.582	81.408	95.576
mixup+CutMix	88.062	88.086	89.390	99.078	90.826	99.246	
MNASNet0_5 (# Params = 2.2 M) (1.6 GFLOPS) ( $N = 16$ )	baseline	67.734	87.49	67.734	87.49	67.734	87.49
	flip	67.690	67.766	68.026	87.632	68.014	87.656
	crop	66.766	66.852	67.082	86.796	66.818	86.746
	affine	60.924	61.028	61.900	83.086	60.600	82.004

Continued on next page

Model	Augmentation	Acc@1	Acc@5	Acc@1	Acc@5	Acc@1	Acc@5
	erasing	67.768	67.846	67.776	87.470	67.706	87.414
	mixup	71.832	71.886	78.968	95.402	82.664	95.974
	CutMix	77.238	77.284	78.938	94.724	79.078	94.514
	flip+crop	66.844	66.926	67.032	86.918	66.964	86.866
	mixup+CutMix	77.254	77.298	80.418	95.804	82.468	96.014
MobileNet_V3_Small (# Params = 2.5 M) (0.96 GFLOPS) ( $N = 16$ )	baseline	67.668	87.402	67.668	87.402	67.668	87.402
	flip	67.646	67.720	67.960	87.668	67.880	87.648
	crop	67.882	67.958	68.236	87.714	68.048	87.590
	affine	65.542	65.632	66.030	85.966	65.552	85.990
	erasing	67.674	67.748	67.720	87.422	67.612	87.416
	mixup	71.734	71.770	78.650	95.072	82.960	96.070
	CutMix	75.028	75.080	76.878	93.684	77.350	93.730
	flip+crop	68.016	68.090	68.156	87.736	68.078	87.714
	mixup+CutMix	76.498	76.552	79.702	95.346	82.330	95.966
ShuffleNet_V2_X0_5 (# Params = 1.4 M) (0.64 GFLOPS) ( $N = 16$ )	baseline	60.552	81.746	60.552	81.746	60.552	81.746
	flip	60.448	60.546	61.376	82.352	61.394	82.470
	crop	60.128	60.230	60.528	81.516	60.372	81.504
	affine	54.350	54.474	55.018	76.736	53.604	75.894
	erasing	60.562	60.666	60.552	81.552	60.514	81.786
	mixup	65.274	65.338	72.124	91.592	77.786	93.506
	CutMix	71.856	71.922	73.696	91.746	74.222	91.622
	flip+crop	60.420	60.512	60.762	81.652	60.554	81.586
	mixup+CutMix	71.116	71.178	74.708	92.590	77.520	93.472
MNASNet0_5 (# Params = 2.2 M) (3.2 GFLOPS) ( $N = 32$ )	baseline	67.734	87.49	67.734	87.49	67.734	87.49
	flip	67.644	67.718	68.050	87.654	68.024	87.670
	crop	66.774	66.858	67.110	86.960	66.892	86.906
	affine	61.386	61.498	62.024	83.178	60.714	82.118
	erasing	67.768	67.846	67.742	87.482	67.726	87.472
	mixup	73.166	73.218	79.676	95.556	83.550	96.384
	CutMix	78.092	78.140	79.554	95.260	79.590	94.796
	flip+crop	66.954	67.034	67.198	86.978	66.990	86.860
	mixup+CutMix	78.588	78.628	81.148	96.036	83.122	96.350
MobileNet_V3_Small (# Params = 2.5 M) (1.92 GFLOPS) ( $N = 32$ )	baseline	67.668	87.402	67.668	87.402	67.668	87.402
	flip	67.584	67.658	57.924	87.670	67.920	87.660
	crop	68.050	68.132	68.288	87.758	68.130	87.686
	affine	65.762	65.836	66.104	86.090	65.668	86.032
	erasing	67.670	67.744	67.684	87.454	67.662	87.408
	mixup	72.956	72.992	79.442	95.208	83.624	96.348
	CutMix	76.050	76.106	77.502	94.052	77.862	93.978
	flip+crop	68.158	68.234	68.302	87.816	68.168	87.664
	mixup+CutMix	77.768	77.802	80.496	95.578	82.964	96.310
ShuffleNet_V2_X0_5 (# Params = 1.4 M) (1.28 GFLOPS) ( $N = 32$ )	baseline	60.552	81.746	60.552	81.746	60.552	81.746
	flip	69.564	60.668	61.354	82.412	61.458	82.482
	crop	60.480	60.576	60.756	81.622	60.526	81.660
	affine	54.804	54.922	55.306	76.920	53.848	76.146
	erasing	60.562	60.666	60.594	81.578	60.568	81.728
	mixup	66.750	66.820	73.140	91.724	78.454	93.776
	CutMix	72.976	73.038	74.362	92.272	74.780	92.204
	flip+crop	60.628	60.734	60.866	81.694	60.746	81.830
	mixup+CutMix	72.634	72.678	75.392	92.970	78.270	93.934

Table 5 reports the detailed StableTTA-I performance shown in Fig. 3 under  $N = 32$ , where the “Peak GFLOPs” column denotes the computational cost of a single forward pass on a  $224 \times 224$  image.

Table 5: Comparison of base models and the StableTTA-I-enhanced models on the ImageNet-1K dataset: model size, computational cost, and top-1 and top-5 validation accuracy.

Weight	Params	Peak GFLOPS	Baseline (%)		StableTTA-I (%)	
			Acc@1	Acc@5	Acc@1	Acc@5
AlexNet [14, 36]	61.1M	0.71	56.522	79.066	89.332	98.028
ConvNeXt_Tiny [18, 36]	28.6M	4.46	82.52	96.146	95.958	99.884
ConvNeXt_Small [18, 36]	50.2M	8.68	83.616	96.65	95.932	99.914
ConvNeXt_Base [18, 36]	88.6M	15.36	84.062	96.87	95.964	99.906
ConvNeXt_Large [18, 36]	197.8M	34.36	84.414	96.976	95.998	99.932
DenseNet121 [10, 36]	8.0M	2.83	74.434	91.972	94.160	99.370
DenseNet161 [10, 36]	28.7M	7.73	77.138	93.56	94.814	99.572
DenseNet169 [10, 36]	14.1M	3.36	75.6	92.806	94.600	99.510
DenseNet201 [10, 36]	20.0M	4.29	76.896	93.37	94.734	99.562
EfficientNet_B0 [33, 36]	5.3M	0.39	77.692	93.532	94.988	99.678
EfficientNet_B1 [33, 36]	7.8M	0.69	78.642	94.186	94.940	99.738
EfficientNet_B2 [33, 36]	9.1M	1.09	80.608	95.31	95.352	99.796
EfficientNet_B3 [33, 36]	12.2M	1.83	82.008	96.054	95.816	99.862
EfficientNet_B4 [33, 36]	19.3M	4.39	83.384	96.594	95.386	99.874
EfficientNet_B5 [33, 36]	30.4M	10.27	83.444	96.628	95.328	99.872
EfficientNet_B6 [33, 36]	43.0M	19.07	84.008	96.916	95.504	99.892
EfficientNet_B7 [33, 36]	66.3M	37.75	84.122	96.908	93.452	99.718
EfficientNet_V2_S [34, 36]	21.5M	8.37	84.228	96.878	96.046	99.926
EfficientNet_V2_M [34, 36]	54.1M	24.58	85.112	97.156	96.102	99.920
EfficientNet_V2_L [34, 36]	118.5M	56.08	85.808	97.788	96.164	99.892
GoogLeNet [31, 36]	6.6M	1.5	69.778	89.53	93.510	99.346
Inception_V3 [32, 36]	27.2M	5.71	77.294	93.45	94.906	99.734
MNASNet0_5 [35, 36]	2.2M	0.1	67.734	87.49	93.122	99.188
MNASNet0_75 [35, 36]	3.2M	0.21	71.18	90.496	93.868	99.484
MNASNet1_0 [35, 36]	4.4M	0.31	73.456	91.51	94.230	99.342
MNASNet1_3 [35, 36]	6.3M	0.53	76.506	93.522	94.876	99.728
MaxVit_T [37, 36]	30.9M	5.56	83.7	96.722	95.996	99.902
MobileNet_V2 [27, 36]	3.5M	0.3	71.878	90.286	93.784	99.262
MobileNet_V2 <sup>†</sup> [27, 24]	3.5M	0.3	72.154	90.822	93.922	99.516
MobileNet_V3_Small [9, 36]	2.5M	0.06	67.668	87.402	92.830	99.094
MobileNet_V3_Large [9, 36]	5.5M	0.22	74.042	91.34	94.350	99.364
MobileNet_V3_Large <sup>†</sup> [9, 24]	5.5M	0.22	75.274	92.566	94.648	99.656
ResNeXt50_32x4d [39, 36]	25.0M	4.23	77.618	93.698	95.126	99.680
ResNeXt50_32x4d <sup>†</sup> [39, 24]	25.0M	4.23	81.198	95.34	95.978	99.916
ResNeXt101_32x8d [39, 36]	88.8M	16.41	79.312	94.526	94.862	99.648
ResNeXt101_32x8d <sup>†</sup> [39, 24]	88.8M	16.41	82.834	96.228	95.764	99.874
ResNet18 [7, 36]	11.7M	1.81	69.758	89.078	93.176	99.194
ResNet34 [7, 36]	21.8M	3.66	73.314	91.42	94.092	99.406
ResNet50 [7, 36]	25.6M	4.09	76.13	92.862	94.518	99.496
ResNet50 <sup>†</sup> [7, 24]	25.6M	4.09	80.858	95.434	95.666	99.866
ResNet101 [7, 36]	44.5M	7.8	77.374	93.546	94.858	99.540
ResNet101 <sup>†</sup> [7, 24]	44.5M	7.8	81.886	95.78	95.804	99.890
ResNet152 [7, 36]	60.2M	11.51	78.312	94.046	95.018	99.558
ResNet152 <sup>†</sup> [7, 24]	60.2M	11.51	82.284	96.002	95.942	99.890
ShuffleNet_V2_X0_5 [21, 36]	1.4M	0.04	60.552	81.746	91.372	98.724
ShuffleNet_V2_X1_0 [21, 36]	2.3M	0.14	69.362	88.316	93.380	99.342
ShuffleNet_V2_X1_5 [21, 36]	3.5M	0.3	72.996	91.086	94.238	99.580
ShuffleNet_V2_X2_0 [21, 36]	7.4M	0.58	76.23	93.006	94.996	99.716
SqueezeNet1_0 [11, 36]	1.2M	0.82	58.092	80.42	89.030	97.878
SqueezeNet1_1 [11, 36]	1.2M	0.35	58.178	80.624	89.642	98.020
Swin_T [16, 36]	28.3M	4.49	81.474	95.776	95.798	99.864
Swin_S [16, 36]	49.6M	8.74	83.196	96.36	95.894	99.914

Continued on next page

Weight	Params	GFLOPS	Acc@1	Acc@5	Acc@1	Acc@5
Swin_B [16, 36]	87.8M	15.43	83.582	96.64	95.832	99.916
Swin_V2_T [17, 36]	28.4M	5.94	82.072	96.132	95.798	99.864
Swin_V2_S [17, 36]	49.7M	11.55	83.712	96.816	96.024	99.902
Swin_V2_B [17, 36]	87.9M	20.32	84.112	96.864	95.890	99.938
VGG11_BN [30, 36]	132.9M	7.61	70.37	89.81	93.542	99.124
VGG11 [30, 36]	132.9M	7.61	69.02	88.628	93.236	99.038
VGG13_BN [30, 36]	133.1M	11.31	71.586	90.374	93.666	99.190
VGG13 [30, 36]	133.0M	11.31	69.928	89.246	93.400	99.084
VGG16_BN [30, 36]	138.4M	15.47	73.36	91.516	93.978	98.242
VGG16 [30, 36]	138.4M	15.47	71.592	90.382	93.542	99.164
VGG19_BN [30, 36]	143.7M	19.63	74.218	91.842	94.122	99.266
VGG19 [30, 36]	143.7M	19.63	72.376	90.876	93.868	99.246
ViT_B_16 [4, 36]	86.6M	17.56	81.072	95.318	95.850	99.886
ViT_B_32 [4, 36]	88.2M	4.41	75.912	92.466	95.000	99.778
ViT_L_16 [4, 36]	304.3M	61.55	79.662	94.638	95.314	99.860
ViT_L_32 [4, 36]	306.5M	15.38	76.972	93.07	95.132	99.804
Wide_ResNet101_2 [41, 36]	126.9M	22.75	78.848	94.284	95.146	99.666
Wide_ResNet101_2 <sup>†</sup> [41, 24]	126.9M	22.75	82.51	96.02	95.914	99.898
Wide_ResNet50_2 [41, 36]	68.9M	11.4	78.468	94.086	95.168	99.654
Wide_ResNet50_2 <sup>†</sup> [41, 24]	68.9M	11.4	81.602	95.758	95.736	99.868

## G Ablation Study of StableTTA-I

Table 6: Ablation studies of StableTTA-I versus TTA under varying numbers of experts ( $N$ ) across multiple architectures. StableTTA-I consistently outperforms TTA under mixup and CutMix.

Model	$N$	GFLOPS	TTA (%)		StableTTA-I (%)	
			Acc@1	Acc@5	Acc@1	Acc@5
AlexNet (# Params = 61.1M)	4	2.84	65.590	87.022	78.750	93.434
	8	5.68	68.604	89.432	84.810	96.216
	16	11.36	70.496	90.510	87.864	97.470
	32	22.72	71.258	90.938	89.532	98.030
ResNet50 <sup>†</sup> (# Params = 25.6M)	4	16.36	88.556	98.858	91.276	99.108
	8	32.72	89.542	99.098	93.878	99.676
	16	65.44	90.232	99.172	95.192	99.800
	32	130.88	90.612	99.240	95.646	99.852
ViT_B_16 (# Params = 86.6M)	4	70.24	87.052	98.470	91.668	99.152
	8	140.48	88.206	98.938	94.042	99.656
	16	280.56	89.048	99.030	95.114	99.820
	32	561.92	89.382	99.074	95.852	99.888
MNASNet0_5 (# Params = 2.2M)	4	0.4	76.806	93.714	85.396	96.614
	8	0.8	79.358	95.276	89.856	98.214
	16	1.6	80.682	95.894	91.882	98.864
	32	3.2	81.162	96.030	93.210	99.222
MobileNet_V3_Small (# Params = 2.5M)	4	0.24	75.716	93.094	85.192	96.392
	8	0.48	78.540	94.664	89.588	97.992
	16	0.96	79.834	95.294	91.770	98.720
	32	1.92	80.552	95.602	92.870	98.998
ShuffleNet_V2_X0_5 (# Params = 1.4M)	4	0.16	70.238	89.682	81.764	94.662
	8	0.32	73.140	91.694	86.936	97.142
	16	0.64	74.536	92.532	90.052	98.358
	32	1.28	75.556	92.898	91.390	98.704

Table 6 reports the detailed performance comparison between standard TTA and our StableTTA-I under mixup and CutMix augmentation policies, across different architectures and varying numbers of experts ( $N$ ). Consistent with the trends observed in Fig. 5a, StableTTA-I outperforms TTA. Larger  $N$  steadily improves both top-1 and top-5 accuracies for all models, including heavyweight models such as AlexNet, ResNet50, and ViT\_B\_16, as well as lightweight models such as MNASNet0\_5, MobileNet\_V3\_Small, and ShuffleNet\_V2\_X0\_5. However, the performance gains gradually plateau as  $N$  increases, indicating a clear saturation effect. This table provides evidences supporting the advantages of StableTTA.

## H Sensitivity Analysis of StableTTA-I

Table 7 presents a detailed sensitivity analysis of StableTTA-I with respect to the number of candidates  $K$  and experts  $N$  across different architectures. Consistent with the trends observed in Fig. 5b, StableTTA-I exhibits strong robustness to the choices of  $K$ , with performance remaining largely stable across a wide range of values. Increasing  $N$  consistently improves both top-1 and top-5 accuracies, while the impact of varying  $K$  is relatively minor. Notably, when logit processing is disabled (when  $K = C$ ), performance drops significantly across all models, reaffirming the critical role of our logit processing (NSS) in achieving accuracy gains. Overall, these results demonstrate that StableTTA-I delivers stable, reliable improvements without requiring meticulous hyperparameter tuning.

Table 7: Sensitivity analysis of StableTTA-I over  $K$  and  $N$ . Results show robustness to  $K$ , consistent gains with larger  $N$ , and significant drops when logit processing is disabled ( $K = C$ ).

Model	$K$	$N = 4$		$N = 8$		$N = 16$		$N = 32$	
		Acc@1	Acc@5	Acc@1	Acc@5	Acc@1	Acc@5	Acc@1	Acc@5
AlexNet (61.1M) (0.71GFLOPS)	1	78.412	93.182	84.638	96.134	87.942	97.530	89.576	98.052
	2	78.444	93.262	84.982	96.312	87.946	97.528	89.496	98.052
	5	78.804	93.328	84.666	96.220	87.984	97.412	89.484	98.108
	10	78.750	93.434	84.810	96.216	87.864	97.470	89.532	98.030
	20	78.540	93.320	84.778	96.160	88.072	97.540	89.530	98.076
	C	66.212	83.420	71.606	91.158	74.948	94.520	76.918	96.222
ResNet50 <sup>†</sup> (25.6M) (4.09GFLOPS)	1	91.524	99.082	93.788	99.614	95.076	99.802	95.706	99.860
	2	91.436	99.120	93.830	99.624	95.022	99.780	95.552	99.834
	5	91.484	99.084	93.746	99.622	94.998	99.818	95.656	99.860
	10	91.276	99.108	93.878	99.676	95.192	99.800	95.646	99.852
	20	91.576	99.126	93.726	99.598	95.008	99.770	95.642	99.876
	C	86.670	96.534	89.820	98.822	92.034	99.542	93.110	99.744
ViT_B_16 (86.6M) (17.6GFLOPS)	1	91.488	99.142	93.906	99.676	95.308	99.822	95.822	99.864
	2	91.604	99.128	94.000	99.670	95.304	99.810	95.826	99.878
	5	91.602	99.112	93.894	99.682	95.088	99.820	95.824	99.884
	10	91.668	99.152	94.042	99.656	95.114	99.820	95.852	99.888
	20	91.468	99.126	94.972	99.648	95.234	99.816	95.940	99.904
	C	86.710	96.578	89.898	98.844	91.648	99.540	92.832	99.744
MNASNet0_5 (2.2M) (0.1GFLOPS)	1	85.416	96.534	89.670	98.222	92.090	98.928	93.060	99.172
	2	85.380	96.450	89.880	98.250	91.900	98.898	93.156	99.190
	5	85.314	96.226	89.842	98.140	92.030	98.854	93.240	99.222
	10	85.396	96.614	89.856	98.214	91.882	98.864	93.210	99.222
	20	85.344	96.500	89.868	98.226	92.124	98.934	93.088	99.178
	C	76.678	90.734	81.654	96.026	84.640	97.886	86.572	98.760
MobileNet_V3_Small (2.5M) (0.06GFLOPS)	1	85.216	96.384	89.566	98.028	91.660	98.712	92.814	99.074
	2	85.356	96.324	89.540	97.988	91.654	98.680	92.818	99.006
	5	85.510	96.480	89.440	97.994	91.762	98.730	92.746	99.014
	10	85.192	96.392	89.588	97.992	91.770	98.720	92.870	98.998
	20	85.290	96.320	89.492	98.014	91.738	98.776	92.774	98.992
	C								

Continued on next page

Model	$K$	Acc@1	Acc@5	Acc@1	Acc@5	Acc@1	Acc@5	Acc@1	Acc@5
	C	76.148	90.256	81.320	95.842	84.176	97.896	86.002	98.664
ShuffleNet_V2_X0_5 (1.4M) (0.04GFLOPS)	1	81.842	94.856	87.246	97.186	89.904	98.274	91.216	98.712
	2	82.136	95.046	87.038	97.178	90.088	98.302	91.326	98.700
	5	81.730	94.694	87.208	97.346	89.868	98.230	91.348	98.674
	10	81.764	94.662	86.936	97.142	90.052	98.358	91.390	98.704
	20	81.492	94.622	87.230	97.314	90.116	98.240	91.426	98.756
	C	71.392	87.140	76.288	93.456	79.464	96.174	81.690	97.606

Additionally, when the batch size is set to 32, the batch boundaries and class boundaries repeat every

$$\text{lcm}(50, 32) = 800,$$

each cycle contains  $800/32 = 25$  batches. Within each cycle, the number of samples from the majority class in each batch follows the pattern:

$$32, 18, 32, 28, 22, 32, 24, 26, 32, 20, 30, 32, 16, 32, 30, 20, 32, 26, 24, 32, 22, 28, 32, 18, 32.$$

The average majority-class ratio is  $672/800 = 84\%$ . In this case, the model performance of both small models (such as MobileNetV2) and stronger models (e.g., ResNet and ViT) decreases by 0.5–1.2% in accuracy compared to the case with batch size 16.

If the batch size is set to 2, 5, 10, 25, or 50 (i.e., any divisor of 50), then each batch lies entirely within a single class. Therefore, every batch is class-pure, and the majority-class ratio is 100%. In this case, even with a batch size of 5 on MobileNetV2, the model accuracy can approach 98%.

## I Means and Standard Deviations of Repeated Experimental Evaluation of StableTTA-I

In Table 8, we report the mean and standard deviation of top-1 and top-5 accuracy on the ImageNet-1K validation dataset for both heavyweight models (e.g., AlexNet, ResNet50, and ViT\_B\_16) and lightweight models (e.g., MNASNet0\_5, MobileNet\_V3\_Small, and ShuffleNet\_V2\_X0\_5) boosted by our StableTTA. Each experiment is conducted independently and repeated five times. The table shows that the standard deviation ranges from approximately 0.01% to 0.1%.

## J Implementation Details of StableTTA-II

Let  $\mathbf{h} \in \mathbb{R}^{C' \times H \times W}$  denote a feature map. The CNN head typically comprises a global average pooling layer followed by a linear layer [18, 10, 33, 35, 27, 9, 39, 7, 21, 41]. The overall computational complexity of the global average pooling layer is:

$$\underbrace{C'(HW - 1)}_{\text{additions}} + \underbrace{C'}_{\text{mean scaling}} = C'HW.$$

The overall computational complexity of a linear layer  $\text{Linear}(C', C)$  is:

$$\underbrace{C'C}_{\text{multiplications}} + \underbrace{(C' - 1)C}_{\text{adds (dot product)}} + \underbrace{C}_{\text{bias adds}} = 2C'C.$$

Table 9 illustrates the feature-level cropping configurations used in StableTTA-II across different architectures. In most model architectures, both the feature height  $H$  and width  $W$  are no larger than 9. Therefore, we typically choose  $k = 1$ , which corresponds to the integer that is closest to removing  $(1 - 224/256)$  proportion size along both the horizontal and vertical directions of the input images. This choice is motivated by the fact that  $k = 1$  is the closest integer such that  $k/9$  approximates  $(1 - 224/256)$ .

It is worth noting that StableTTA-II cannot be replaced with weighted features:

$$\frac{1}{N} \sum_{i=1}^N \text{Head}(\text{Crop}^{(i)}(\mathbf{h})) \neq \text{Head}\left(\frac{1}{N} \sum_{i=1}^N \text{Crop}^{(i)}(\mathbf{h})\right).$$

Table 8: ImageNet-1K validation accuracy (Top-1/Top-5). Mean and standard deviation are reported over five independent runs for both heavyweight and lightweight models.

	AlexNet (%)		ResNet50 <sup>†</sup> (%)		ViT_B_16 (%)	
	Acc@1	Acc@5	Acc@1	Acc@5	Acc@1	Acc@5
	89.492	98.034	95.596	99.862	95.888	99.868
	89.558	98.056	95.622	99.854	95.830	99.898
	89.642	98.020	95.620	99.868	95.916	99.896
	89.620	98.070	95.684	99.842	95.848	99.882
	89.588	98.096	95.666	99.858	95.876	99.878
mean	89.580	98.055	95.638	99.857	95.872	99.884
std	0.059	0.030	0.036	0.010	0.034	0.013
	MNASNet0_5		MobileNet_V3_Small		ShuffleNet_V2_X0_5	
	Acc@1	Acc@5	Acc@1	Acc@5	Acc@1	Acc@5
	93.014	99.256	92.772	99.004	91.222	98.686
	93.092	99.212	92.784	99.060	91.334	98.750
	93.288	99.204	92.746	99.052	91.370	98.764
	93.090	99.208	92.896	99.000	91.128	98.690
	93.138	99.262	92.882	99.032	91.314	98.772
mean	93.124	99.228	92.816	99.030	91.274	98.732
std	0.103	0.026	0.070	0.026	0.099	0.039

Although some model heads consist primarily of global average pooling followed by a linear layer, the above equation holds if and only if the model head is linear that contains only a global average pooling layer followed by a linear layer without bias or activation functions.

## K Extra Experiments of StableTTA-II

Flipping and 90-degree rotations are not valid transformations at the feature level because CNN classification heads typically begin with a global average pooling layer, which enforces invariance to such operations:

$$\text{AvgPool}(\psi(\mathbf{h})) = \mathbf{h}, \quad \psi \in \{\text{Flip}, \text{Rotation}_{90}, \text{Rotation}_{180}, \text{Rotation}_{270}\}.$$

In this appendix, we evaluate several cropping strategies:

- TripleCrop: identity + horizontal center + vertical center
- FiveCrop: identity + left + right + top + bottom
- SevenCrop: identity + left + right + top + bottom + horizontal center + vertical center
- NineCrop: identity + left + right + top + bottom + top-left + top-right + bottom-left + bottom-right

We also introduce RandomCrop( $p$ ), where  $p$  denotes the probability of sampling from the set of eight spatial crops (left, right, top, bottom, and four corners). This sampling is repeated 8 times, and the identity crop is always appended to ensure at least one valid (non-empty) selection.

Additionally, we consider Random Erasing, which randomly masks feature-level pixels with probability  $p$  before feeding them into the model head.

Fig 10 illustrates the sensitivity of model performance to different cropping strategies and random erasing probabilities.

Table 9: Feature-level cropping configurations used in StableTTA-II across different architectures.

Model	Head	Crops
ConvNeXt_Tiny	AvgPool+Norm+Linear(768,1000)	$h, h_{1:-1,:}, h_{:,1:-1}, h_{:,1:-1}$
ConvNeXt_Small	AvgPool+Norm+Linear(768,1000)	$h, h_{1:-1,:}, h_{:,1:-1}, h_{:,1:-1}, h_{:,1:-1}$
ConvNeXt_Base	AvgPool+Norm+Linear(1024,1000)	$h, h_{1:-1,:}, h_{:,1:-1}, h_{:,1:-1}, h_{:,1:-1}$
ConvNeXt_Large	AvgPool+Norm+Linear(1536,1000)	$h, h_{1:-1,:}, h_{:,1:-1}, h_{:,1:-1}, h_{:,1:-1}$
DenseNet121	ReLU+AvgPool+Linear(1024,1000)	$h, h_{1:-1,:}, h_{:,1:-1}$
DenseNet161	ReLU+AvgPool+Linear(2208,1000)	$h, h_{1:-1,:}, h_{:,1:-1}$
DenseNet169	ReLU+AvgPool+Linear(1664,1000)	$h, h_{1:-1,:}, h_{:,1:-1}$
DenseNet201	ReLU+AvgPool+Linear(1920,1000)	$h, h_{1:-1,:}, h_{:,1:-1}$
EfficientNet_B0	AvgPool+DropOut+Linear(1280,1000)	$h, h_{1:-1,:}, h_{:,1:-1}, h_{1:-1,1:-1}$
EfficientNet_B1	AvgPool+DropOut+Linear(1280,1000)	$h, h_{1:-1,:}, h_{:,1:-1}, h_{1:-1,1:-1}$
EfficientNet_B2	AvgPool+DropOut+Linear(1408,1000)	$h, h_{1:-1,:}, h_{:,1:-1}, h_{1:-1,1:-1}$
EfficientNet_B3	AvgPool+DropOut+Linear(1536,1000)	$h, h_{2:-2,:}, h_{:,2:-2}, h_{2:-2,2:-2}$
EfficientNet_B4	AvgPool+DropOut+Linear(1792,1000)	$h, h_{2:-2,:}, h_{:,2:-2}, h_{2:-2,2:-2}$
MNASNet0_5	AvgPool+DropOut+Linear(1280,1000)	$h, h_{1:-1,:}, h_{:,1:-1}$
MNASNet0_75	AvgPool+DropOut+Linear(1280,1000)	$h, h_{1:-1,:}, h_{:,1:-1}$
MNASNet1_0	AvgPool+DropOut+Linear(1280,1000)	$h, h_{1:-1,:}, h_{:,1:-1}$
MNASNet1_3	AvgPool+DropOut+Linear(1280,1000)	$h, h_{1:-1,:}, h_{:,1:-1}$
MobileNet_V2	AvgPool+DropOut+Linear(1280,1000)	$h, h_{1:-1,:}, h_{:,1:-1}, h_{1:-1,1:-1}$
MobileNet_V3_Small	AvgPool+Linear(576,1024)+Hardswish+DropOut+Linear(1024,1000)	$h, h_{1:-1,:}, h_{:,1:-1}, h_{1:-1,1:-1}$
MobileNet_V3_Large	AvgPool+Linear(960,1280)+Hardswish+DropOut+Linear(1280,1000)	$h, h_{1:-1,:}, h_{:,1:-1}, h_{1:-1,1:-1}$
ResNeXt50_32x4d	AvgPool+Linear(2048,1000)	$h, h_{1:-1,:}, h_{:,1:-1}$
ResNeXt101_32x8d	AvgPool+Linear(2048,1000)	$h, h_{1:-1,:}, h_{:,1:-1}$
ResNeXt101_64x4d	AvgPool+Linear(2048,1000)	$h, h_{1:-1,:}, h_{:,1:-1}$
ResNet18	AvgPool+Linear(512,1000)	$h, h_{1:-1,:}, h_{:,1:-1}$
ResNet34	AvgPool+Linear(512,1000)	$h, h_{1:-1,:}, h_{:,1:-1}$
ResNet50	AvgPool+Linear(2048,1000)	$h, h_{1:-1,:}, h_{:,1:-1}$
ResNet101	AvgPool+Linear(2048,1000)	$h, h_{1:-1,:}, h_{:,1:-1}$
ResNet152	AvgPool+Linear(2048,1000)	$h, h_{1:-1,:}, h_{:,1:-1}$
ShuffleNet_V2_X0_5	AvgPool+Linear(1024,1000)	$h, h_{1:-1,:}, h_{:,1:-1}, h_{1:-1,1:-1}$
ShuffleNet_V2_X1_0	AvgPool+Linear(1024,1000)	$h, h_{1:-1,:}, h_{:,1:-1}, h_{1:-1,1:-1}$
ShuffleNet_V2_X1_5	AvgPool+Linear(1024,1000)	$h, h_{1:-1,:}, h_{:,1:-1}, h_{1:-1,1:-1}$
ShuffleNet_V2_X2_0	AvgPool+Linear(1024,1000)	$h, h_{1:-1,:}, h_{:,1:-1}, h_{1:-1,1:-1}$
Wide_ResNet50_2	AvgPool+Linear(2048,1000)	$h, h_{1:-1,:}, h_{:,1:-1}$
Wide_ResNet101_2	AvgPool+Linear(2048,1000)	$h, h_{1:-1,:}, h_{:,1:-1}$

## L Additional Discussion on Addressing the Computational Cost of Ensemble Methods

It is worth noting that nearly all CNNs accept dynamically sized input images. Therefore, one possible solution to reduce the computational cost of TTA is to resize the augmented images to a lower resolution. However, this idea does not work well in practice. For example, we randomly apply 10-crop to a raw  $224 \times 224$  image, producing 10 individual images with resize resolutions of  $224 \times 224$ , and then resize all of them to  $112 \times 112$  before feeding them into MobileNetV2. In this

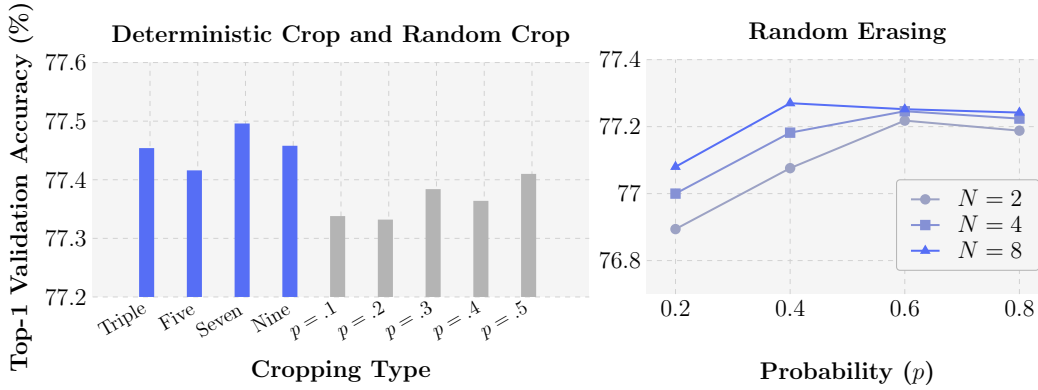


Figure 10: **Sensitivity analysis of cropping strategies and random erasing.** Left: Comparison of deterministic multi-crop methods (TripleCrop, FiveCrop, SevenCrop, NineCrop) and RandomCrop with varying probabilities  $p$ . Right: Effect of Random Erasing probability  $p$  on top-1 validation accuracy for different numbers of experts  $N \in \{2, 4, 8\}$ . Overall, moderate cropping diversity improves performance, while excessive randomness provides degraded returns.

way, the computational cost of each inference is reduced, but the final validation accuracy drops from 71.878% to 55.816%.

Another unintuitive fact is that ImageNet-1K models usually resize images to  $256 \times 256$  and then apply center cropping to obtain  $224 \times 224$  images for standard validation. If we keep the full image and directly resize it to  $224 \times 224$ , the validation accuracy becomes worse than the baseline. Both phenomena are easy to verify and reproduce.

Now let us reconsider why people do not split a large image into patches as model inputs and then aggregate the final outputs to reduce the computational cost of each forward pass. For example, we can divide a  $224 \times 224$  image into four  $112 \times 112$  patches and sum the corresponding logits from the four patches. However, this idea also does not work well. Our experiments show that, for MobileNetV2, the final validation accuracy drops from 71.878% to 62.780%.